Investigation of the Effects of Histone H3.3 Mutations in Craniofacial Development

Nadine Nzirorera

Department of Human Genetics
Faculty of Medicine
McGill University, Montreal, Quebec, Canada
March 2021

A thesis submitted to the Faculty of Graduate and Postdoctoral Studies in partial fulfillment of the requirements of the degree of Master of Science.

DEDICATION

This thesis is dedicated to my family. Especially to my late father, Innocent Nzirorera. Though you are no longer with us, your memory continues to inspire and your belief in me made this possible. I miss you more than words can express. To my beloved mother, Josephine Uwamaryia and my siblings, Carine Nzirorera, Alex Nzirorera and Chris Nzirorera; you mean the world to me and I thank you for the lifetime of support.

ABSTRACT

Histone proteins are not only fundamental to both the structural integrity and organization of DNA but play a fundamental role in gene expression, and craniofacial development is an intricate process that requires the coordinated expression of many genes. With evidence of histone h3.3 incorporation in nucleosomes being important in the development of cranial neural crest cell derived cartilage and bone, as well as the recent discovery of human patients with *de novo* germline missense mutations in histone H3.3 encoding gene *H3F3A* presenting with craniofacial abnormalities, suggests there is a role of histone H3.3 in cranial neural crest cells (NCCs), the main contributors in craniofacial development. Whether there is a cell-type specific requirement of H3.3 in NCCs and proper craniofacial development has not previously been explored.

Here, we use CRISPR/Cas9 to generate a mouse model and mate it with *Wnt1-Cre2* transgenic mice to express a missense mutation (H3.3-G34R) in neural crest cells. Alcian Blue and Alizarin Red staining was used in embryonic day (E) 14.5 and 17.5 embryos to assess craniofacial cartilage and bone formation, respectively. We found:

I) Embryos expressing the H3.3-G34R mutation only in neural crest cells showed no difference between control mice.

II) Constitutive expression of H3.3-G34R resulted in reduction of NCC-derived cartilages and decreased ossification in NCC-derived head bones of E14.5 and E17.5 embryos.

III) E17.5 *H3f3a*-Null embryos showed severe ossification defects in NCC and mesoderm derived head bones.

Our data suggests that the expression of H3.3-G34R specifically in neural crest cells does not affect craniofacial development in mice. Additionally, moderate to severe reduction of NCC-derived cartilage and bone, seen in constitutive H3.3-G34R and *H3f3a*-null embryos respectively, supports constitutive expression of H3.3-G34R as well as removal of H3.3A partially inhibits craniofacial cartilage and bone formation. Additional analyses such as RNAseq and ChIPSeq are needed to assess if there are any transcriptomic differences or changes in H3.3 post-translational modification in mutants compared to control mice, allowing discovery of possible genes and pathways leading to these phenotypes.

RÉSUMÉ

Les protéines histones sont non seulement fondamentales à l'intégrité structurale et l'organisation de l'ADN, mais sont aussi des acteurs majeurs dans l'expression des gènes et le développement craniofacial. Le development craniofacial est un processus complexe qui nécessite l'expression coordonnée de nombreux gènes. Avec la preuve de l'incorporation de l'histone h3.3 dans les nucléosomes étant importante dans le développement du cartilage et de l'os dérivés des cellules de la crête neurale crânienne, ainsi que la découverte récente de patients humains avec des mutations faux-sens *de novo* de la lignée germinale dans l'histone H3.3 codant *H3F3A* présentant une anomalies craniofaciales, suggèrent qu'il existe un rôle de l'histone H3.3 dans les cellules de la crête neurale crânienne (CCN), les principaux contributeurs au développement craniofacial. La question de savoir s'il existe une exigence spécifique de type cellulaire de H3.3 dans les CCN et un développement craniofacial approprié n'a pas été explorée auparavant.

Dans cette recherche, on a crée un modèle de souris conditionnel et l'on a accouplé avec des souris transgéniques *Wnt1-Cre2* pour exprimer une mutation faux-sens (H3.3-G34R) dans les cellules de la crête neurale. La coloration au bleu Alcian et au rouge Alizarien a été utilisée dans les embryons provenant d'embryons de jour (E) 14,5 et 17,5 pour évaluer respectivement le cartilage craniofacial et la formation osseuse. Les données trouvées:

I) Les embryons exprimant conditionnellement la mutation H3.3-G34R dans les cellules de la crête neurale n'ont montré aucune différence entre les souris témoins.

II) L'expression constitutionnelle de H3.3-G34R a entraîné une réduction des cartilages dérivés du CCN et une diminution de l'ossification dans les os de la tête dérivés du NCC d'embryons E14.5 et E17.5.

III) Les embryons E17.5 *H3f3a*-Null présentaient de graves défauts d'ossification dans les os de la tête dérivés du CCN et du mésoderme.

Nos données suggèrent que l'expression conditionnelle de cellules H3.3-G34R dans de la crête neurales n'affectent pas le développement de craniofaciale dans les souris. La réduction modérée à sévère du cartilage et de l'os dérivés de la CCN observée dans les embryons constitutifs H3.3-G34R et *H3f3a*-null, respectivement, soutient l'expression constitutive de H3.3-G34R ainsi que l'élimination de H3.3A inhibe partiellement le cartilage craniofacial et la formation osseuse. Les analyses supplémentaires telle que RNAseq et ChIPSeq sont nécessaires

pour évaluer s'il existe des différences transcriptomiques ou des changements dans la modification post-traductionnelle H3.3 chez les mutants par rapport aux témoins, permettant la découverte de gènes et de voies possibles menant à ces phénotypes.

TABLE OF CONTENTS

LIST OF ABBREVIATIONS

AP	Anterior-Posterior
BMP	Bone Morphogenetic Protein
bp	Base pairs
DIPG	Diffuse Intrinsic Pontine Glioma
Dll	Distal-less
ChIPSeq	Chromatin immunoprecipitation sequencing
E	Embryonic Day
EGF	Epidermal Growth Gactor
EMT	Epithelial to Mesenchymal Transition
ESCs	Embryonic Stem Cells
ET-1	Endothelin-1
FGF	Fibroblast Growth Factor
FISH	Fluorescence in Situ Hybridization
FNP	Frontonasal Prominence
G	Generation
GCTB	Giant Cell Tumor of the Bone
HDR	Homology Directed Repair
HMTs	Histone Methyltransferases
LLS	Luscan-Lumish syndrome
NCCs	Neural Crest Cells
NSD1	Nuclear Receptor Binding SET Domain Protein 1
PcG	Polycomb Group
PRC1	Polycomb repressive complex 1
PRC2	Polycomb repressive complex 2
PTMs	Post-Translational Modifications
RNAseq	Ribonucleic acid sequencing
SAM	S-Adenosyl methionine

SETD2	SET Domain Containing 2
Shh	Sonic Hedgehog
TF	Transcription Factor
tg	Transgene
TGFα	Transforming Growth Factor Alpha
TGFβ	Transforming Growth Factor β
TrxG	Trithorax-group
Wnt	Wingless

LIST OF FIGURES

LIST OF TABLES

ACKNOWLEDGMENTS

I had the pleasure of being a part of an exceptional lab group that made my masters extremely special and I am thankful. Thank you, **Dr. Loydie A. Jerome-Majewska** for the opportunity to join your lab group, for your encouragement, unwavering support, seemingly endless patience and for rekindling my love of running. Thank you to **Dr. Marie-Claude Beauchamp** for your grounded perspective, shared goofy sense of humor and maintaining a positive and lighthearted lab environment any graduate student could ever hope for. **Dr. Jean-François Boisclair Lachance**, thank you for your kind and accommodating nature, vast knowledge (never failing to answer all of my questions) and plethora of corny jokes I will miss. Thank you, **Sabrina Shameen Alam**, for your wise words in both science and in life. I will cherish them forever and there is no one I'd rather be a "loser" with after 8pm. **Shruti Kumar**, my government-allotted quarantine bubble buddy and one of my greatest friends, I will always appreciate your love of exploration and taking me along for the ride. **Rachel Aber**, thank you for making my time during this masters an absolute blast, filled with lifetime memories. I hope to be able to visit you soon. Thank you, **Maryam**, for all your support, putting up with me as a roommate and agreeing to force each other to exercise during quarantine. Although it was brief, we meant well. Thank you, **Cal**, **Elias**, and **Nargess** for all the laughs and late-night memes and thank you to my best friend, **Victor,** for visiting whenever you could throughout this journey, and reminding me of home. Thank you to **Dr. Nada Jabado** and **Dr. Nikoleta Juretic** for your expertise, support and providing me with the means to obtain my masters. Thank you to **Dr. Livia Garcia**, **Dr. Denny Dufort** and once again **Dr. Nada Jabado**, for being on my committee and guiding me throughout this journey. Lastly, I would like to give thanks to the extremely knowledgeable members and collaborators of the Jabado lab, including **Dr. Augusto Faria Andrade**, **Caterina Russo**, **Dr. Damien Faury**, **Dr. Sima Khazaei**, **Dr. Carol Chen**, **Mitra Cowan** and **Jade Desjardins**.

FORMAT OF THESIS

This thesis follows the traditional format and includes five chapters. Chapter I is the introduction, comprised of a literature review, rationale, hypothesis, aims and objectives. Chapter II contains the methods for each previously stated aim. Chapter III contains the study results, Chapter IV contains the discussion, and lastly Chapter V contains future directions.

CONTRIBUTION OF AUTHORS

This thesis was written by the candidate and experiments performed were done with the assistance of members of the Dr. Loydie Jerome-Majewska and Dr. Nada Jabado lab. The abstract for the project was translated into French by Josephine Uwamaryia. The study was funded by the Jabado lab, through received grants from the Canadian Institutes of Health Research (CIHR), Genome Canada, and the National Institute of Mental Health (NIH). The Jabado lab was also responsible for the inspiration to create novel transgenic mouse lines that express mutant H3.3 mutations implicated in pediatric bone and brain cancers. The use of mouse lines to explore the role of H3.3 in craniofacial development, through mating with *Wnt1-Cre2* transgenic mice, was inspired by the candidate. There are three figures in this thesis that were not created by the candidate. Figure 1.5 is a public domain illustration, adopted from Wikipedia. Figure 1.6 and 1.7 were created by the candidate's lab (Jerome-Majewska). Lastly, part of Figure 3.13 (illustrating neural crest cell and mesoderm derived mouse head bones) was adopted from Cibi et al. 2017 upon the author's approval. All other figures within this thesis were created by the candidate.

Generation of mouse lines

The G34W repair template plasmid was designed and synthesized by the Livia Garcia, Nada Jabado and Loydie Jerome-Majewska lab groups. The candidate performed all mutagenesis experiments to synthesize additional repair templates (G34R, G34V, WT, G34W, K27M, K36M). CRISPR/Cas9 microinjections to give rise to founder lines were done by collaborator, Mitra Cowan. PCR program/condition troubleshooting, and design were created by candidate to genotype novel mouse lines. Sanger sequencing preparation for validation of both repair templates and mouse lines (PCR, gel extractions, cloning, bacterial transformation, primer design, miniprep, plate preparation, alignment) were performed by candidate.

Characterizing the role of histone H3.3 in craniofacial development

Animal facility housing of the H3.3-G34R murine colony was funded by the Jerome-Majewska lab. Maintenance of the colony, specifically the mating, routine weaning, genotyping and euthanasia of mice, was done by the candidate. In addition, the experiments described for the characterization of H3.3-G34R in craniofacial development (dissections, embryo collection, cartilage preparations, skeletal preparations, and image analysis) were also performed by the candidate.

CHAPTER I: INTRODUCTION

Histone proteins and epigenetics

Eukaryotes possess genomic DNA that is quite lengthy and must be effectively condensed and packaged in order to fit within a single cell. DNA packaging is facilitated through its association with basic proteins called histones (Figure 1.1). Roughly 147 base pairs of DNA are tightly coiled around octameric complexes composed of two copies of each of the four core histone proteins: H2A, H2B, H3, and H4. The octamer consists of two H2A-H2B dimers that are surrounded by an H3-H4 tetramer and they form the nucleosome core. This nucleosome core associates with histone H1, which is bound to 60-80 base pairs of DNA, referred to as "linker DNA", between nucleosomes (Figure 1.2). Histone H1 is a stabilizer histone, which works to pack the nucleosome octamer together (Kalashnikova et al., 2016).

Nucleosomes exist in repeating units and can be seen resembling beads on a string under the microscope. These repeating units make up chromatin, the basis of the higher order packaging structure we know as chromosomes (Kornberg, 1974; Luger et al., 1997; Thomas and Kornberg, 1975; Tremethick, 2007). Regulating how tightly packed nucleosomes are in a given region of chromatin is one way that differential gene expression is achieved. Genes located in regions of DNA more tightly packed by histones are concealed and shielded from transcription factors (TF), therefore making them transcriptionally silent. Alternatively, genes located in loosely packed DNA, are more accessible to TF binding and primed for transcription (Field et al. 2008).

Heterochromatin and euchromatin

Chromatin states are often referred to as either euchromatic or heterochromatic. When chromatin is in a heterochromatic state, nucleosomes are tightly packaged together and are transcriptionally repressed. Euchromatin is composed of more loosely packed nucleosome repeats and is transcriptionally active. Heterochromatin can be either "constitutive", where it is unwavering and remains transcriptionally inactive, or "facultative", where it can be altered through certain epigenetic chemical modifications to be made euchromatic (Passarge 1979; Allshire & Madhani, 2019).

Epigenetics is defined as heritable and reversible modifications to nucleotide bases or chromosomes that do not change the genome, or specific sequence of nucleotides, but can alter gene expression (Waddington, 1942; Wolffe & Matzke, 1999; Handy et al., 2012). Epigenetic programming allows for the same genome to have different patterns of expression contingent on

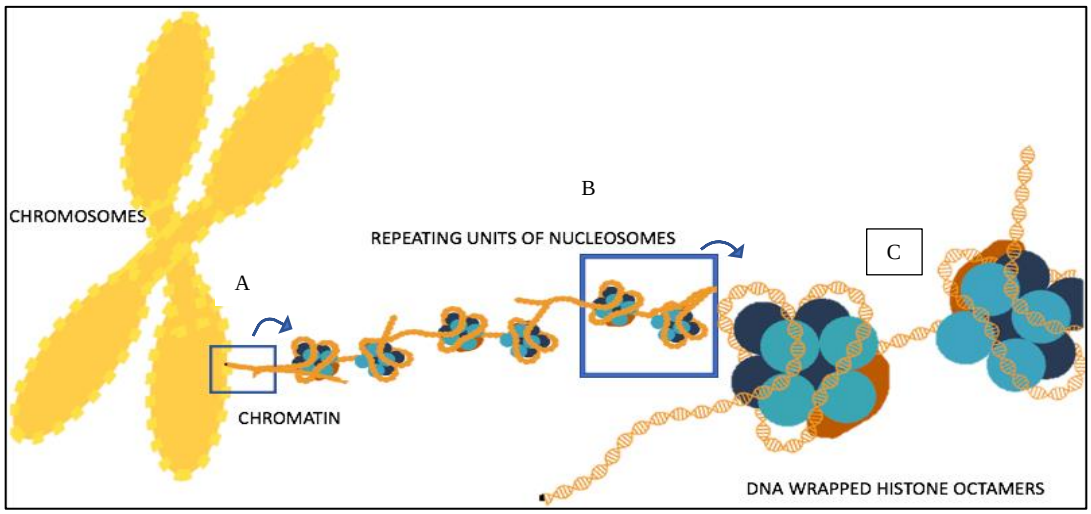

Figure 1.1: Hierarchy of DNA packaging. The chromosome is made up of chromatin (A). Chromatin is composed of repeating units of nucleosomes (B). Nucleosomes are composed of DNA wrapped around a histone octamer (C).

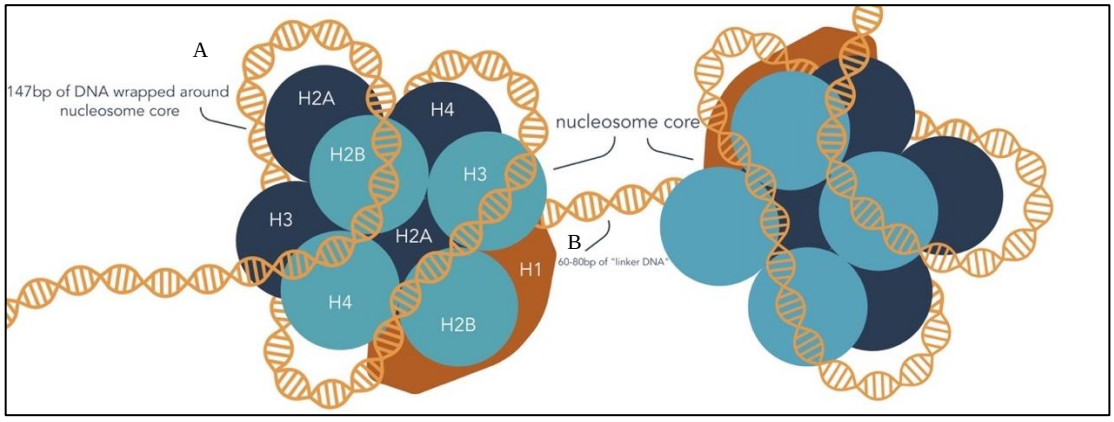

Figure 1.2: The nucleosome core. Nucleosomes are histone octamers wrapped in 147 base pairs of DNA. The histone octamer is composed of two copies of each of the four core histone proteins H2A, H2B, H3 and H4 (A). Octamers are packaged by histone variant H1, connected to each other by 60-80bp of DNA coined “linker DNA” (B).

alterations to the chromatin, further contributing to the complexity and potential of the cell (Handy et al., 2012). The modification of histone tails is one example of an epigenetic mechanism that occurs within the cell. Chromatin can be made more transcriptionally active or repressed when chemical modifications are added to histone tails (Alberts, 2002; Handy et al.,

2012). These modifications are called post-translational modifications (PTMs). A majority of PTMs occur on the amino acid residues of the N-terminal tail of histone proteins (Furukawa et al. 2020) (Figure 1.3). Modifications involve the addition or removal of chemical groups to the histone proteins, through help of enzymes called histone writers and erasers, respectively. A few PTMs include DNA acetylation, methylation, phosphorylation and ubiquitylation. Depending on the histone modification, DNA can become more or less tightly wound to histones, either easing or restricting the accessibility of TFs to DNA and regulating the accessibility and expression of genetic information (Alberts, 2002). The effect a PTM has on the transcriptional activity of chromatin (whether activating or repressing) varies with the residue that is modified and cell type. Simply put, addition of a certain chemical group can be transcriptionally activating in some cellular contexts and transcriptionally repressing in others. Some examples of chemical group modifications and their general **(**not definitive**),** effect on transcription are listed in Table 1.1).

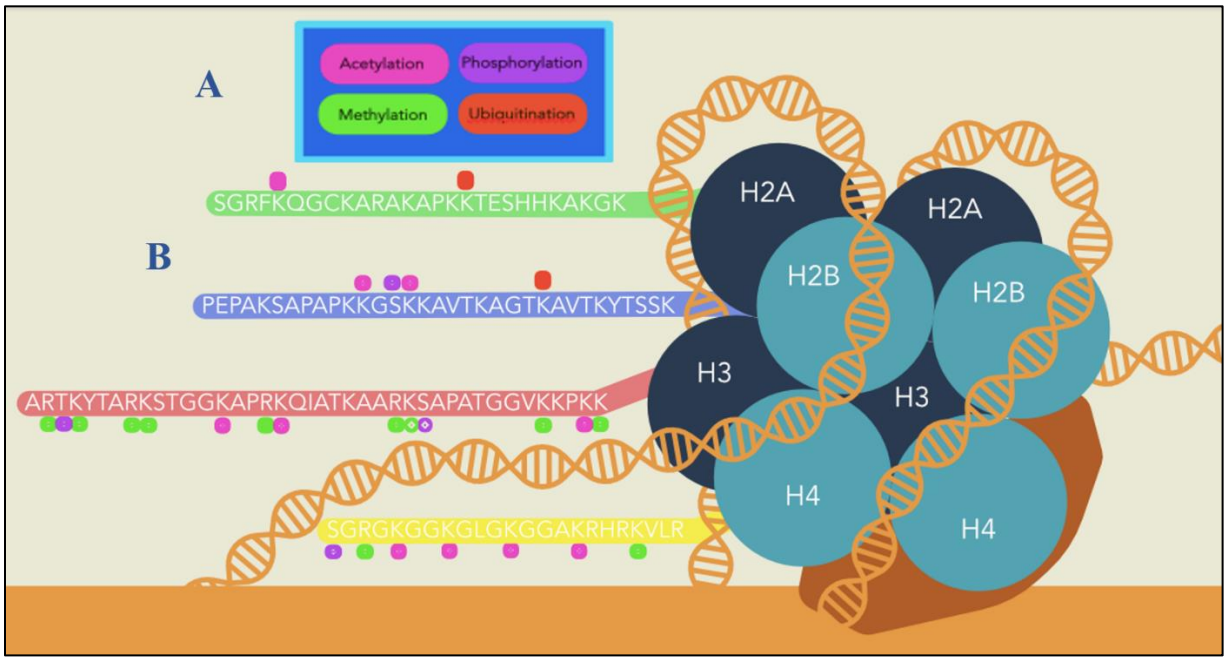

Figure 1.3: Post-translational modifications that can occur on specific residues of the N-terminal tails of histone variants H1, H2, H3, and H4. Examples of PTMs are acetylation (in pink), phosphorylation (in purple), methylation (in green), and ubiquitination (in red) (A). The N-terminal tails of the four core histone proteins are modified on specific amino acid residues. Examples of specific residues that are post-translationally modified are: acetylation, methylation, phosphorylation and ubiquitination (B). Modifications are indicated by a block with their respective color (color code shown in “A”).

Table 1.1: Histone modifications and their general effect on the transcriptional activity of chromatin.

Modification	General Effect on Transcriptional Activity
Acetylation	Activation
Ubiquitination	Repression
Methylation	Both Activation and Repression
Phosphorylation	Activation

Histone modifiers and histone H3

Three types of enzymes play a role in establishing the histone modifications necessary for the cell by catalyzing the transfer of chemical groups. These enzyme classes are coined histone writers, readers, and erasers (Gilette et al., 2016). Histone writers are responsible for adding chemical groups to histone tails, histone readers have "reading" capabilities able to detect and bind to particular modifications, and histone erasers act to remove modifications deposited on histone tails (Simo-Riudalbas et al., 2015). Each post-translational modification – whether it's acetylation, methylation, phosphorylation, etc. – has its own class of enzymatic writers, readers and erasers. Some histone writers exclusively modify a specific site or residue of the histone N-terminal tail, while other writers catalyze modifications on multiple sites of the histone tail (Bannister, 2011). The most extensively modified site of all histones occurs on the N-terminal tails of the histone variant histone H3 (Xu et al. 2014). The most studied H3 modification is the methylation of its lysine (K) residues by histone methyltransferases (HMTs). With the discovery of mutations in both H3 writers and in histone H3 proteins themselves, specifically in a variant of histone H3 called histone H3.3, being implicated in human diseases and disorders, the study of histone H3.3 has become an area of great interest and is the main focus of this study.

The histone H3 variant "histone H3.3"

Histone H3 is one of the main four histones that comprise the nucleosome core. There are five variants of H3 in total: the main variants H3.1, H3.2, and H3.3 as well as two other variants specific to the centromere and testes, CENP-A and H3t, respectively. Two of the three main variants, H3.1 and H3.2 are canonical, with ten genes encoding histone H3.1 and three genes encoding H3.2. Canonical H3.1 and H3.2 expression is cell cycle-coupled, with their genes organized in intron-less clusters designed for rapid expression and allowing for the quick

assembly of nucleosomes during DNA synthesis. Histone H3.3, however, is unique because it is a replication-independent variant, meaning its expression can occur both during the cell cycle as well as independently/outside of the cell cycle (Bramlage, 1997). Histone H3.3 is encoded by the genes *H3F3A* and *H3F3B. H3F3A* is located on chromosome 1 (1q42.12) and *H3F3B* is located on chromosome 17 (17q25.1). Deposition of H3.3 is commonly found in euchromatic as well as heterochromatic regions of the mammalian genome (Bush, 2013).

Histone H3 modification by histone methyltransferases

Histone H3 HMTs catalyze the deposition of methyl groups on basic residues such as lysine (K) and arginine (R). For this study, I will provide an overview on the methyl modification of the H3 N-terminal tail lysine residues, lysine 36 (H3K36), lysine 27 (H3K27), and lysine 4 (H3K4), which are supported to be important in various developmental processes (Greer & Shi, 2012). Humans possess at least eight HMTs responsible for either mono, di, or tri-methylation of H3K36. These enzymes all have a catalytic domain in common called Su(var)3-9, Ez, Trithorax or "SET" which utilizes the cofactor S-Adenosyl methionine (SAM) to transfer methyl groups to histone tails (Zheng et al. 2012; Zhao et al. 2015). One of the eight HMTs SET Domain Containing 2 or SETD2, solely tri-methylates (deposits three methyl groups) H3K36. Modification of H3K36 has been shown to be involved in the processes of transcriptional repression, sex-chromosome dosage compensation, DNA replication, recombination and repair. Trimethylation of H3K36, specifically, has also been found to be important in splicing (Zaghi et al., 2020). NSD1 is another histone H3K36 methyltransferase which primarily di-methylates the H3K36 residue (Qiao et al. 2011) and is thought to modulate the H3K27 methyltransferase Polycomb repressive complex 2 (PRC2), by delineating genome-wide H3K27me2 and H3K27me3 domains in embryonic stem cells (ESCs) (Streubel et al., 2018).

Polycomb group proteins are a set of enzymes that work to transcriptionally silence genes and are divided into two groups, Polycomb repressive complex 1 (PRC1) and Polycomb repressive complex 2 (PRC2). Both groups are multi-subunit protein complexes that work to mono, di, and tri methylate H3K27. PRC1 is able to inhibit RNA polymerase II preinitiation complex assembly and ubiquitylates histone H2A, promoting gene silencing. PRC2 is responsible for the trimethylation of H3K27, through association with the catalytic subunit EZH2. Deposition on this mark is thought to serve multiple functions vital to cell survival and

development, such as X-chromosome inactivation, PRC2-mediated suppression of Hox genes, animal body patterning, and pluripotent maintenance of embryonic stem cells.

Another group of methyltransferases are the Trithorax-group (TrxG) proteins. TrxG proteins specifically methylate H3K4. H3K4 can be mono, di or trimethylated and each mark (in both plants and animals) is commonly found in euchromatic regions of DNA and associated with actively transcribed genes (Sims et al., 2003). H3K4 methylation is seen at promoter regions and transcription start sites and its trimethylation (H3K4me3) is of high interest due to its role in the maintenance of stem cell properties in eukaryotes (Benayoun et al., 2014; Hyun et al., 2017).

Embryonic stem cells harbor high numbers of domains with both trimethylation of H3K4 and H3K27, a property not seen in more differentiated cells. These marks are considered "antagonistic" in that H3K4me3 is associated with active transcription while H3K27me3 is associated with transcriptional repression (Sims et al., 2003). Sites containing these antagonistic marks have been coined "bivalent" or "poised" domains and they are thought to play a functional role in upholding pluripotency. Maintenance of pluripotency is proposed to occur through the simultaneous repression of developmental transcription factors by H3K27me3 while H3K4me3 ensures that future upregulation of genes can occur at the time they will be necessary for development and differentiation (Mikkelsen et al., 2007). As mentioned, H3K27 and H3K4 trimethylation is regulated by the Polycomb (PcG) and Trithorax (TrxG) protein families, respectively. Isolation of PcG and TrxG proteins was initially performed in *Drosophila* and found to be important in governing the expression of HOX genes, genes which encode highly conserved transcription factors, whose spatially restricted expression defines the anterior-posterior (AP) axial identity in metazoans (Shah et al., 2010).

Mutations of histone H3.3 in human conditions

A hallmark of tumor cells is an aberration of PTMs, such as hypomethylation of lysine residues. This is thought to be the reason why mutations in modifying enzymes are implicated in various human cancers because they inhibit proper PTM deposition. In addition, multiple pediatric cancers have been associated with recurrent *de novo* missense mutations in the gene *H3F3A*, which cause amino acid substitutions in the N-terminal tail of histone H3.3. Mutations occur on or near the key sites of modification, H3K27 and H3K36. For example G34R/V, in which glycine at residue 34 is substituted by arginine (G34R) or valine (G34V), is implicated in pediatric glioblastoma. Additionally, K27M, entailing a lysine substitution to methionine on the

27th residue of the histone tail, is implicated in brainstem cancer diffuse intrinsic pontine glioma (D.I.P.G) (Schwartzentruber et al., 2012; Wu et al., 2012) (Figure 1.4). Later on, two additional point mutations, K36M and G34W/L, were implicated in the bone tumors chondroblastoma and giant cell tumor of the bone (GCTB), respectively (Behjati et al., 2013). The G34W/L mutation in histone H3.3 entails the substitution of glycine to tryptophan or leucine in the 34th position of the H3.3 tail, and the K36M mutation involves substitution of lysine to methionine in the 36th position of the histone H3.3 tail (Behjati et al., 2013) (Figure 1.4).

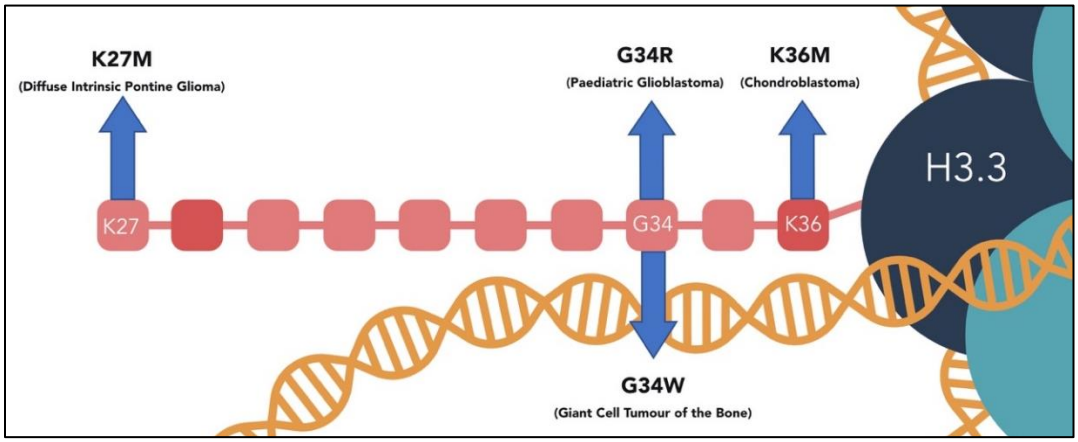

Figure 1.4: Somatic missense mutations in the N-terminal tail of histone H3.3 are found in pediatric bone and brain tumors. The histone H3.3 K27M mutation is associated with diffuse intrinsic pontine glioma (D.I.P.G), G34R is implicated in paediatric glioblastoma, G3W in giant cell tumor of the bone, and K36M in chondroblastoma.

My research interests lie in craniofacial development and this will be focus of this thesis. Mutations in H3 remodelling enzymes cause a variety of human syndromes that present with craniofacial abnormalities (Imaizumi et al., 2002; Kurotaki et al., 2002; Luscan et al., 2014; Lumish et al., 2015; van Rij et al., 2018). These syndromes fall into a class of syndromes called overgrowth syndromes, characterized by either a generalized or localized overgrowth of tissues; additional phenotypes include macrocephaly (abnormally large head), a tall stature, neurodevelopmental delay, and craniofacial abnormalities (Brioude, 2019). Microdeletions in *NSD1* was identified as the cause of Sotos syndrome (Sotos et al., 1964; Douglas et al., 2003; Rio et al. 2003). Constitutive missense mutations and small intragenic deletions and insertions in *EZH2*, are reported to cause Weaver syndrome, and Luscan-Lumish syndrome (LLS) is caused

by heterozygous point mutations or deletions in *SETD2* (Luscan et al., 2014; Lumish et al., 2015; van Rij etal., 2018).

A variety of craniofacial abnormalities present across these syndromes. In Sotos syndrome, features include long narrow face, macrocephaly with large prominent forehead, and long/broad chin (Cole & Hughes, 1994). LLS patients present with large prominent forehead, long nose, prominent lower jaw and malar hypoplasia (reduction in facial cheek bones). Finally, Weaver syndrome phenotypes include macrocephaly, large ears, retrognathia (abnormal posterior positioning of the lower jaw), long philtrum, dimpled chin, and widely spaced eyes (Kamien et al., 2018; Gibson et al., 2012; Taton-Brown & Rahman, 2013; Luscan et al., 2014). In addition, constitutive heterozygous mutations in H3.3 have recently been found in patients with developmental disorders and present with craniofacial abnormalities (Maver et al., 2019; Bryant et al., 2020).

Patients with mutations in H3 remodellers or histone H3.3 present with a range of phenotypes

Exome sequencing of a five-year-old female patient with severe neurodevelopmental delay of unknown cause revealed a *de novo* heterozygous missense mutation in *H3F3A*. The mutation was a leucine to arginine amino acid substitution in the 62nd position of H3.3 (L62R). At the age of 5 she was unable to walk or speak and presented with both cranial and cardiac defects including microcephaly, hypertelorism (widely spaced eyes), facial hypotonia (reduced muscle tone), poorly formed low set ears, wide and depressed nasal bridge, and hypoplasia (reduction) of the corpus callosum and cerebellum. Lastly, cardiac defects included a non-life threatening, though atypical, atrial septum. This study was a case report, only reporting on a single patient, but was first in identifying germline heterozygous mutations in *H3F3A* (Maver et al., 2019). Later, exome and genome sequencing done on patients with neurodevelopmental delays and/or cognitive defects identified 46 additional patients with *de novo* heterozygous germline mutations in *H3F3A* or *H3F3B* (Bryant et al., 2020). Mutations were spread throughout the coding sequence of both genes and there was no genotype-phenotype correlation with respect to the location of the mutation in both genes. None of these patients had cancer but shared phenotypes of both undergrowth and overgrowth, developmental/neurological delays and congenital anomalies.

Neurologic/developmental phenotypes included patients taking significantly longer on average to achieve developmental milestones such as independent sitting (ranging from 6 months

to seven years), walking (15 months to 8 years), and speaking (12 months to 6 years). Neurological diseases showed progression and included cortical atrophy, seizures, hypotonia, spasticity, contracture (muscle stiffening), and oculomotor abnormalities (hindrance in the ability to move the eye). Patients also exhibit craniofacial abnormalities such as a high prominent forehead, hypertelorism (widely spaced eyes), craniosynostosis (premature fusion of skull during infancy causing a misshapen skull), and plagiocephaly (also known as flat head syndrome where one side of the skull is flattened). Cardiac abnormalities were also found such as atrial septal defects, and additional phenotypes included abnormal skeletal formation, abnormal genital formation and chronic constipation.

Presence of germline mutations in *H3F3A* in patients who present with both craniofacial and cardiac development abnormalities, suggests an importance of *H3F3A*-encoded histone H3.3 in craniofacial development (Bryant et al., 2020). To provide a better understanding of the potential role of H3.3 in craniofacial development, I will quickly go over craniofacial morphogenesis followed by previous findings on the role of histone H3.3 in development.

Summary of craniofacial development

Neural crest cells are a population of migratory cells arising from the margins between the ectoderm and the neural plate and are fundamental contributors to the craniofacial skeleton. It is after neurulation in which NCCs from the roof plate, or dorsal midline of the neural tube, undergo epithelial to mesenchymal transition (EMT) (Srinivasan & Toh, 2019) (Figure 1.5). During EMT they delaminate from the neuroepithelium and migrate outwards to populate the pharyngeal arches (Morrison et al., 2017) of the developing embryo. Once their final destinations are reached, the NCCs differentiate, yielding a range of tissues such as melanocytes, endocrine cells, neurons, myofibroblasts, glial cells, cartilage and bone (William et al., 2001).

The processes in NCC development are achieved through a complex of regulatory genes, signaling pathways and factors that equip the NCCs with their multipotency and migratory capabilities, as well as control their patterning and differentiation. Factors arise directly from NCCs, facilitating communication between them, as well as from proximal cells of ectodermal, endodermal or mesodermal origins.

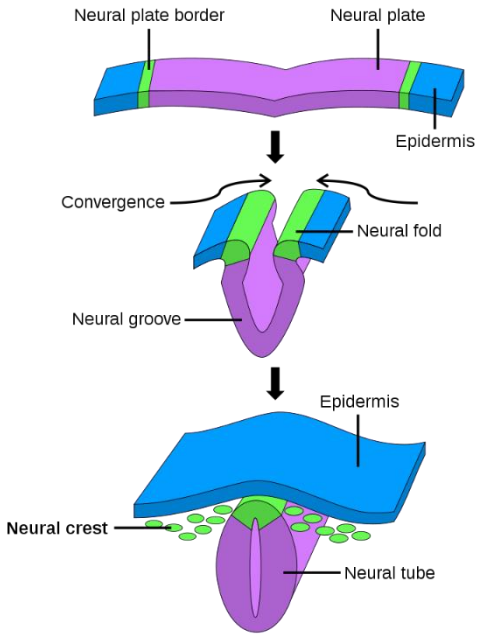

Figure 1.5: The process of neural tube closure and neural crest cell delamination.
The neural plate borders or neural folds (green) converge. The neural plate (purple) first forms the neural groove and then becomes the neural tube. Neural crest cells (NCC) arise from the neural plate border ectoderm (green) located underneath the ectoderm (blue) and undergo epithelial to mesenchymal transition, migrating dorsolaterally and delaminating from the neural tube. These NCC precursors then go on to differentiate into a multitude of cell types (Public domain illustration from Wikipedia).

It is as early as the fourth week of human embryonic development, after gastrulation and subsequent establishment of the primary germ layers and notochord, where presence of the first pharyngeal arch signifies the start of craniofacial development. Pharyngeal arches are paired structures that form along the foregut of the developing embryo, situated below the developing brain, and look like small bulb-like protrusions. The five paired pharyngeal arches are composed of a combination of the primary germ layers with a mesodermal core, lined internally with endoderm and externally by the ectoderm derived neural crest cells, equipped to form the variety of cell types needed for formation of the head and neck. The facial prominences form around the primitive mouth in the fourth week of human embryonic development and give rise to the developing the face. The five facial prominences include a single frontonasal prominence and paired maxillary and mandibular prominences. The frontonasal prominence (FNP) includes two

processes called the medial nasal process (which gives rise to the middle of the nose) and the lateral nasal process (which gives rise to the terminal lateral ends of the nose) (Figure 1.6).

The FNP is predominately neural crest cell derived and gives rise to the forehead, nose, part of the upper lip and primary palate. The paired maxillary and mandibular prominences form the midface and lower face respectively; with the maxillary prominences forming the upper lip as well as the secondary palate. Fusion of the maxillary prominences with the frontal nasal prominence then forms the philtrum, the vertical groove located between the bottom of the nose and upper lip (Peter & Larsen, 2004; Ansari & Bordoni, 2019). Finally, the mandibular prominences form the mandible, or lower jaw, as well as a portion of the tongue. The eyes have ectodermal, mesenchymal, as well as neural crest origins and are initially situated laterally on the head, but as development progresses, move to their conventional anterior position of the head (Ansari & Bordoni, 2019).

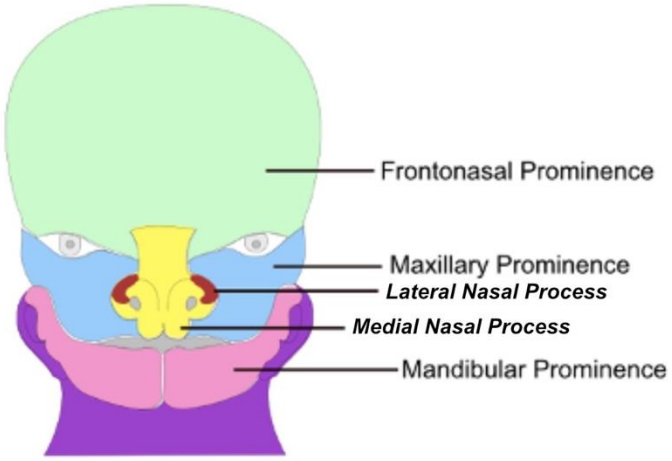

Figure 1.6: The five facial prominences. Humans form five facial prominences: two paired maxillary prominences (blue), two paired mandibular prominences (pink) and finally the frontonasal prominence (green) that includes two processes; the lateral nasal process (red) and medial nasal process (yellow). (Figure adopted from Jerome-Majewska lab).

The vertebrate skull is categorized into two distinct regions, the neurocranium and the viscerocranium. The neurocranium is of mixed paraxial mesoderm and neural crest cell origins. The neurocranium includes the protective skull, encapsulating the brain and sense organs and the parietal, frontal, occipital, sphenoid and temporal bones, all of which form through

intramembranous ossification. The viscerocranium encompasses the facial skeleton and is entirely neural crest cell derived, giving rise to the mandible, maxilla, palatine bones, bones of the nose, zygomatic bones, dentine of the teeth and the bones of the ear (Kuratani, 2018; Wilkie, 2001; Knight & Schilling, 2013).

Craniofacial development is homologous in mice and humans

Although various vertebrate models have contributed tremendously to our understanding of craniofacial development, the mouse model is a particularly suitable organism to study human craniofacial development because it reflects human head morphogenesis very closely (Wilkie & Morriss-Kay, 2001; Otterloo et al., 2017) with mice developing the same five facial prominences that humans do (Figure 1.7).

Figure 1.7: Homology of craniofacial development in mice and humans. Mouse craniofacial morphogenesis involves the formation of the same facial prominences formed in humans. Homologous structures between mouse and human are highlighted by the same color. Facial prominences include the frontonasal prominence (green and yellow), paired maxillary prominences (blue), and paired mandibular prominences (pink). Developmental age in which each stage of craniofacial development occurs is displayed. Starting at 4 weeks in humans and embryonic day 9.5 in mice. (Figure adopted from Jerome-Majewska lab).

Neurocristopathies

Aberration in NCC development can lead to neurocristopathies. Neurocristopathies are any disorders that arise from defects in any aspect of neural crest cell biology (Bolande, 1974). Improper migration of this transient embryonic cell population, or inability to properly respond

to environmental signals within the migrating population, can all result in abnormal specification, and/or differentiation in neural crest cells and lead to neurocristopathies. Neurocristopathies occur in approximately 1 in 700 live births and encompass many diseases and syndromes that fall on a broad spectrum of severities (Yoon et al., 2016). Since NCCs are the main contributors to craniofacial bone and cartilage, a common feature of neurocristopathies is craniofacial abnormalities. Some examples of craniofacial abnormalities are microcephaly or macrocephaly (small head or large head) and hypoplasia/aplasia (the underdevelopment/absence of development) of facial elements. Neurocristopathies can also include deafness and heart defects, as NCCs give rise to the auditory bones, the malleus, incus and stapes as well as cardiac structures, such as the outflow tract of the heart.

The role of histone H3.3 in development

Various studies support the variant histone H3.3 as elemental for cell division and genome integrity. In *Drosophila*, independent loss of homologous H3.3 coding genes, *His3.3A* or *His3.3B,* had no effect on development. Total loss of H3.3 protein however, through double knockout of *His3.3A* and *His3.3B,* resulted in reduced viability and infertility, with H3.3 ablation impairing chromosomal segregation, resulting in meiotic defects in cells (Hodl & Basler, 2009; Sakai et al. 2009). Depletion of H3.3 in *Xenopus* leads to developmental arrest in late gastrulation, causing defects such as failure of blastopore closure and increased cell death (Szenker et al., 2012). Analysis of mouse zygotes showed that H3.3 assists in a genome-wide remodelling of chromatin, and upon H3.3 depletion using a morpholino, processes such as DNA replication and transcription were severely reduced (Lin et al., 2014).

Mice have two genes, *H3f3a* and *H3f3b,* which code for identical H3.3 protein, homologous to humans. Mixed results have been found in the phenotypes of *in vivo* mouse models (Table 1.2). While a more recent study reported that knockout mice of either gene, *H3f3a* or *H3f3b*, are overtly normal and fertile (Jang et al., 2015), others have found that *H3f3a* ablation (*H3f3a* $^{-/-}$) led to growth deficiency (Tang et al., 2015) and showed evidence of embryonic lethality and infertility (Bush et al., 2013). Single allelic gene trap of *H3f3b* (*H3f3b*$^{-/+}$) were reported to be growth deficient, and males were sterile (Tang et al., 2015). *H3f3b* knockouts (*H3f3b*$^{-/-}$) have also been reported to be semi-lethal, causing perinatal mortality; with *in vitro* analysis showing defective cell division and chromosome segregation (Bush et al., 2013). Complete removal of H3.3, through knockout of both *H3f3a* and *H3f3b,* triggers cell cycle

suppression and cell death in early embryogenesis with a high rate of mortality occurring during the pre-implantation stage at embryonic day 4.5 (E4.5) (Jang et al., 2015). H3.3 depletion *in vitro* resulted in mitotic defects such as lagging chromosomes and anaphase bridges, and upon further analysis with fluorescence in situ hybridization (FISH), dicentric chromosomes were detected as a result of telomeric fusions (Jang et al., 2015). Together these studies support that H3.3 is crucial to a variety of cellular and developmental processes, including support of chromosomal structure, suggesting H3.3 plays a role in the maintenance of genome integrity during mammalian development (Tang et al., 2015; Jang et al., 2015).

Table 1.2: Summary of phenotypes seen in generated *H3f3a* and *H3f3b* knockout mouse models.

Genotype	**Genetic Background**	**Mutation Mechanism**	**Phenotypes**	**Reference**
H3f3a $^{+/-}$	C57BL/6 and 129	Gene trap targeting vector in intron 1 causing exon 2 deletion (Null/knockout, Reporter)	Normal	(Jang et al., 2015)
	129 Sv/Ev	Retroviral gene trap vector integrated into intron 1	Normal	(Couldrey et al., 1999)
	129S1/SvImJ (129S1)	Targeted allele (deletion of *H3f3a* coding sequence)	Normal	(Tang et al., 2015)
	BALB/c	Deletion of *H3f3a* exons 2 to 4 (floxed)	Normal	(Bush et al., 2013)
	129S1/SvImJ 129S4/SvJaeSor	Targeting vector replaced part of exon 2	Normal	(Tang et al., 2013)

H3f3b $^{+/-}$	C57BL/6 and 129	Gene trap targeting vector in intron 1 causing exon 2 deletion (Null/knockout, Reporter)	Normal	(Jang et al., 2015)
	129S1/SvImJ (129S1)	Targeted allele (deletion of *H3f3b* coding sequence)	Male sterility	(Tang et al., 2015)
H3f3a $^{-/-}$	C57BL/6 and 129	Gene trap targeting vector in intron 1 causing exon 2 deletion (Null/knockout, Reporter)	Normal	(Jang et al., 2015)
	129S1/SvImJ	Targeting vector replaced part of exon 2	Normal, some growth deficient	(Tang et al., 2013)
	129 Sv/Ev	Retroviral gene trap vector with lacZ/neo fusion gene, integrated into the first intron of the gene.	Reduced fertility, neonatal lethality, postnatal growth delay, abnormal grip strength	(Couldrey et al., 1999)
	BALB/c	Deletion of *H3f3a* exons 2 to 4 (floxed)	Embryonic lethality and infertility	(Bush et al., 2013)
	129S1/SvImJ (129S1)	Targeted allele (deletion of *H3f3a* coding sequence)	Male subfertility, Growth deficiency at weaning age	(Tang et al., 2015)

H3f3b $^{-/-}$	C57BL/6 and 129	Targeted allele, exon 2 deletion (Null/knockout, Reporter)	Normal	(Jang et al., 2015)
	BALB/c	Deletion of *H3f3a* exons 2 to 4 (floxed)	Semi-lethal with Perinatal mortality	(Bush et al., 2013)

Histone H3.3 in craniofacial development

There has only been one animal model study which specifically investigates the effect of missense mutations in histone H3.3 in craniofacial development. In this study, an N-ethyl-N-nitrosourea (ENU) mutagenesis screen led to identification of mutant zebrafish lacking neural crest cell derived head cartilage, bone and teeth. Microsatellite mapping revealed that mutant zebrafish contained a missense mutation in *h3f3a*, specifically an amino acid substitution of aspartic acid to asparagine (D123N), near the C terminus of the histone core domain. To validate *h3f3a* as causative for zebrafish mutant phenotypes, mRNA encoding mutant H3.3 was injected into one-cell stage zebrafish and compared to wildtype h3.3 controls. While wildtype H3.3 mRNA injected zebrafish were unaffected, mutant h3.3 mRNA zebrafish recapitulated the original phenotype and lacked cranial neural crest cell derived head skeleton. The skeletal phenotype of mutants resembled previously generated compound mutant *tfap2a;foxd3* zebrafish (Wang et al., 2011), which lack all cranial NCC-derived tissues. *tfap2a* and *foxd3* are early genes expressed during gastrulation and are essential for neural crest cell induction (Wang et al., 2011). Phenotypic similarities of *tfap2a;foxd3* compound mutants with D123N mutants suggest that missense mutations in *h3f3a* may affect expression of early genes necessary for cranial neural crest cell development. Through nuclear fractionation it was found that the mutant H3.3 D123N was under-enriched in purified nucleosomes compared to wildtype H3.3, and more importantly, displayed a dominant-negative effect by forming aberrant associations with wild-type H3.3. These aberrant associations resulted in a severe reduction of wildtype H3.3 being incorporated into nucleosomes. Absence of solely neural crest cell derived head cartilages and bones in mutant zebrafish, as a consequence of the depletion of H3.3 in nucleosomes, suggests that the NCC population is particularly sensitive to reduced levels of H3.3; hindering their induction,

and, in turn, their ability to give rise to the cell types necessary for vertebrate head development (Cox et al., 2012).

The general consensus through *in vivo* and *in vitro* studies is that histone H3.3 is fundamental to the structural integrity and organization of DNA; essential to cell division, maintenance of genome integrity and development. Previous studies support that missense mutations in H3.3 affect craniofacial development (Cox et al., 2012). Furthermore, the existence of human patients with germline missense mutations in H3.3 coding genes, who present with craniofacial abnormalities, suggest there may be a requirement for H3.3 in neural crest cell development (Maver et al., 2019; Bryant et al., 2020). These studies, however, report on the constitutive expression of mutated H3.3, which begs the question, "is there a cell-type specific requirement of histone H3.3 in neural crest cells?". It would be interesting to study the effects of mutated H3.3-G34R when expressed specifically in the neural crest cells themselves; serving to further clarify the role of H3.3 in craniofacial development.

Collaboration and the H3.3- G34R mutation

Since the discovery of somatic missense mutations in H3.3 being associated with the development of pediatric tumors of the bone and brain (Swartzentruber et al., 2012; Wu et al., 2012; Behjati et al., 2013), the Jabado lab had the desire to generate six different lines of mutant mice that would allow for temporal and cell-type specific expression of each of the recurrent mutations found in H3.3, which includes G34R, G34V, G34W, K27M, K36M and a wildtype line for comparison. Mouse models would incorporate the Cre/l*ox* system, able to express mutant H3.3 in a cell-type specific manner, through mating with *Cre* transgenic mouse lines. With this, we collaborated with the Jabado lab to achieve the two goals of this project: 1) Generate all five of the knock-in mutant H3.3 mouse lines, representing the mutations found in previously described pediatric cancers (G34R, G34V, G34W, K27M, K36M) as well as a sixth wildtype control mouse line. And 2) Utilize one of the mutant lines to mate to *Wnt1-Cre2* transgenic mice and express mutant H3.3 in neural crest cells, allowing us to explore if that specific H3.3 mutation in NCCs disrupts craniofacial development.

The first mutant line generated was the H3.3-G34R mouse line and this is why it was selected for this study.

HYPOTHESIS

We propose that there is a cell-type specific requirement for histone H3.3 in neural crest cells for their proper development and subsequent craniofacial morphogenesis. We hypothesize that when we mate mutant *H3f3a*$^{LoxP/+}$ mice with *Wnt1-Cre2* transgenic mice to drive expression of the H3.3-G34R missense mutation in NCCs, it will affect NCC migration and/or differentiation and in turn cause craniofacial abnormalities in embryos.

AIMS

To address the hypothesis that there is a cell-type specific requirement for histone H3.3 in neural crest cells and craniofacial development, I have established three aims.

AIM I: Generate five different plasmids each carrying one of the H3.3 missense mutations.

AIM II: Identify founder mice with the desired mutation.

AIM III: Express H3.3-G34R in the neural crest cells and assess craniofacial development.

OBJECTIVES

AIM I

To generate the various repair templates needed to generate our lines of conditional mutant mice, there was a single objective:

1) Perform quick-change site directed mutagenesis to give rise to G34R, G34V, K27M, K36M and wildtype H3.3 encoding repair templates.

AIM II

To identify founder mice with our mutation of interest I had two objectives:

1) Design primers and PCR program to genotype and confirm correct locus insertion of the construct in G1 pups born from CRSIPR/Cas9 generated G0 founder mice.

2) Sanger sequence the PCR products to validate that all components of the construct are intact and the CRISPR/Cas9 microinjections were successful.

AIM III

For my aim to express H3.3-G34R in neural crest cells and analyze the effects on craniofacial development, the following objective was established:

1) Mate our conditional *H3f3a*$^{LoxP/+}$ (H3.3-G34R) mutant line with *Wnt1-Cre2* transgenic mice to express H3.3-G34R in NCCs and characterize cartilage and bone formation of E14.5 and E17.5 mutants and create a robust genotyping system to identify embryos of all genotypes.

The following chapter with describe the materials and methods for Aims I, II, and III.

CHAPTER II: MATERIALS & METHODS

AIM I

Repair template design

A plasmid construct/repair template carrying the H3.3-G34W point mutation (c.103G>T, p.Gly35Trp) was used. The construct was composed of a 400-base pair (400bp) 5' homology arm followed by a splice acceptor, GFP cassette, and poly A tail floxed by LoxP sequences. After the second LoxP, there is a 422bp mutant cDNA sequence encoding the full open reading frame for *H3f3a* (*H3f3a* exons 2, 3 and 4). Exon 2 is where the point mutation resides. The mutant cDNA is then followed by a second poly A sequence and 400bp 3' homology arm (Figure 2.1).

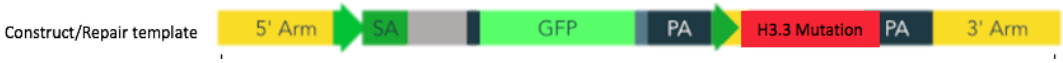

Figure 2.1: Plasmid construct/repair template design. Repair template is composed of a 5' homology arm ("5' Arm" in yellow), followed by a splice acceptor (SA), GFP reporter (GFP), poly A tail (PA) floxed by LoxP sequences (green arrows) and downstream cDNA containing mutant H3.3 (red), followed by second PolyA (PA) and 3' homology arm ("3' Arm" in yellow).

Quick change site-directed mutagenesis

The plasmid carrying the H3.3-G34W mutation (c.103G>T, p.Gly35Trp) was used as a backbone to mutate a single base pair and give rise to the five other plasmids carrying the other H3.3 mutations: G34R, G34V, K27M, K36M, as well as a wildtype H3.3 encoding construct. The quick-change protocol was adapted from the "*QuikChange II Site-Directed Mutagenesis Kit"* (Cat No./ID: #200524). For the mutagenesis, 33 bp long forward and reverse primer pairs (Table 2.1), complementary to the opposite strands of the vector, were ordered from the *Thermofisher's* Custom DNA Oligos Synthesis service.

Table 2.1: Forward and reverse primers used in quick change mutagenesis with mutated base pair is indicated in bold.

Mutation	**Primer**	**Mutation Standard Notation**
G34R	Forward: GCG CCC TCT ACT GGA **A**GG GTG AAG AAA CCT CAT	c.103G>A p.Gly35Arg

	Reverse: ATG AGG TTT CTT CAC CC**T** TCC AGT AGA GGG CGC	
G34V	Forward: GCG CCC TCT ACT GGA G**T**G GTG AAG AAA CCT CAT Reverse: ATG AGG TTT CTT CAC C**A**C TCC AGT AGA GGG CGC	c.104G>T p.Gly35Val
Wildtype	Forward: GCG CCC TCT ACT GGA GGG GTG AAG AAA CCT CAT Reverse: ATG AGG TTT CTT CAC CCC TCC AGT AGA GGG CGC	c.103G p.Gly35
K27M	Forward: ACA AAA GCC GCT CGC A**T**G AGT GCG CCC TCT ACT Reverse: AGT AGA GGG CGC ACT C**A**T GCG AGC GGC TTT TGT	c.83A>T p.Lys28Met
K36M	Forward: TCT ACT GGA GGG GTG A**T**G GTG AAG AAA CCT CAT Reverse: ATG AGG TTT CTT CAC C**A**T CAC CCC TCC AGT AGA	c.110A>T p.Lys37Met

The G34R and G34V were generated first as the desired point mutation to be introduced were located at the same position. Then the wildtype repair template was generated, and it was used as a backbone to generate the K36M and K27M repair templates. Mutagenesis was carried out by setting up the following reaction mix in a single well of a standard 8-well PCR strip tube (Table 2.2).

Table 2.2: Reaction mix used in quick change mutagenesis

Reagent	**Volume (uL)**
Repair Template Backbone (50 ng/uL)	1
10× Cloned *Pfu* DNA polymerase reaction buffer (Cat No.: 200532)	5
Forward Primer (100ng/uL)	1
Reverse Primer (100ng/uL)	1
Invitrogen dNTP Mix (Cat No.: 18427013) (10mM)	1
Agilent *PfuTurbo* DNA Polymerase (Cat No.: 600250)	1
ddH2O	40

The master mix was then placed in the following PCR program (Table 2.3). After the PCR step, 1uL of *Dpn1* (*New England BioLabs* Cat No.: R0176S) was added to the reaction and incubated at 37^{o}C for 90 minutes to digest the parental repair template DNA.

Table 2.3: PCR program used in quick change mutagenesis

Temperature	**Time**	
95^{o}C	1 minute	
95^{o}C	**50 seconds**	X **18 cycles**
60^{o}C	**50 seconds**	
68^{o}C	**3 minutes**	
68^{o}C	7 minutes	
4^{o}C	hold	

Cloning of quick-change products

After parental repair template digestion, PCR products were cloned into the pCRTM2.1-TOPO® vector by following the The *Life Technologies TOPO TA Cloning Kit Transform One Shot*® manual (Publication #: MAN0000047, page 13).

Bacterial transformation and liquid cultures of quick-change products

Vectors containing quick-change products were then transformed into XL1-blue competent cells and plated on ampicillin treated agar plates. Ten colonies were picked and cultured for 16 hours, overnight, as detailed in the *Life Technologies TOPO TA Cloning Kit Transform One Shot® Life* manual (Publication #: MAN0000047, page 19).

Miniprep

Minipreps were performed from liquid cultures by following the "*Molecular cloning: a laboratory manual" Plasmid DNA Extraction* protocol (Sambrook & Fritsch & Maniatis, 1989). Minipreps were resuspended in 20ul of TE Buffer (pH=8.0).

Designing primers to sequence for mutation

Primer3 was used to design the following primers to Sanger sequence cDNA in generated plasmids for desired mutation (Table 2.4).

Table 2.4: Primers generated for Sanger sequencing validation of H3.3 mutant plasmids

Primer Name	**Sequence (5' to 3')**
cDNAseq1	CCAACCAGATAGGCCTCACT
cDNAseq2	CTAGCTGGATATCTTTTGGCA
cDNAseq3	TTAAGCACGTTCTCCGCGTATGC
cDNAseq4	CAACGAGCGGATCCAGAC
cDNAseq5	AACGAGCGGATCCAGACA
Sequencing-3-F	GGGCCGGGCGGCCGGTGTCG
Sequencing-Mutation-F	TTTCCAGATTTGGGGG
F-GFP-cDNA1	CGACAACCACTACCTGAGCA
F-GFP-cDNA2	CCACTACCTGAGCACCCAGT
F-GFP-cDNA3	CCCGACAACCACTACCTGAG

F-GFP-cDNA4	CCGACAACCACTACCTGAGC
R-GFP-CDNA	TGCGGATCAGAAGTTCAGTG

Sanger sequencing of quick-change repair templates

Isolated plasmids were verified to confirm that the intended point mutation was introduced through Sanger sequencing. A volume of 10ul of template plasmid was sent for sequencing with Primer3 designed reverse primer, "R-GFP-CDNA" (5'-TGCGGATCAGAAGTTCAGTG-3'), ordered from Thermofisher. The primer flanked the cDNA region and was 60-90bp downstream from the mutant base pair.

Maxi prep

After Sanger sequencing verification, a plasmid with the correct point mutation was chosen, and its respective liquid culture was used for maxi prep following the QIAGEN® Plasmid Maxi Kit (Cat No./ID: 12165) protocol for large scale preparation.

AIM II, OBJECTIVE I

CRISPR/Cas9

CRISPR/Cas9 mediated insertion of all plasmid templates through microinjections of two-cell staged zygotes were done by collaborator, Mitra Cowen. Zygotes were transferred to pseudo pregnant mixed background C57B/6-C3H recipient females to give rise to founder lines.

Overview of construct function

Each construct functioned as a promoter trap insertion with the endogenous *H3f3a* promoter intended to drive its expression (Friedel & Soriano, 2017). Designed gRNAs direct *Cas9* mediated cleaving of intron 1 in the *H3F3A* locus (Figure 2.2A) and the 5' and 3' homology arms promote homology directed repair (HDR) (Figure 2.2B). Upon HDR and insertion into the targeted locus, GFP expression is driven by the endogenous *H3f3a* promoter and mice will fluoresce green when screened through florescence (Figure 2.2C). There is a poly A sequence following GFP (and upstream of the mutant H3.3 cDNA) that should inhibit further transcription downstream, meaning no transcription or translation of mutant cDNA or endogenous *H3f3a*

exons 2, 3 and 4 should occur (Figure 2.2C). This creates a null allele, making mice with a single allelic insertion hemizygous for *H3f3a* (which has been confirmed to be non-lethal in mice). In this state, these mice are denoted as "*H3f3a*$^{LoxP/+}$" or HEMI-H3.3A. The knock-in H3.3 mutation is only expressed upon *Cre*-mediated recombination when mated with transgenic *Cre* mice. *Cre*-mediated recombination causes excision of the GFP reporter and the first polyA. The endogenous *H3f3a* promoter will now drive expression of the mutant histone H3.3 cDNA (Figure 2.2D).

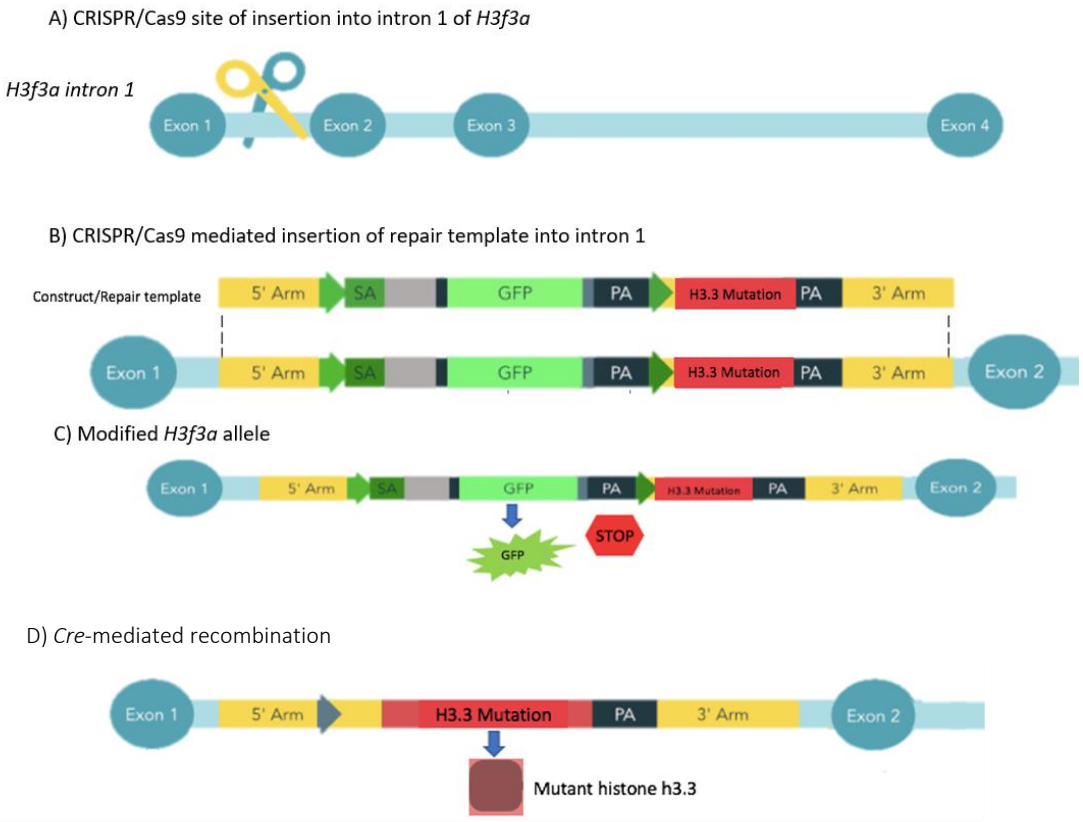

Figure 2.2: Mechanism of action of the repair template. Cas9 cleaving will occur in intron 1 of the *H3f3a* locus (A). Homology directed repair will assist in its incorporation into intron 1 (B). Construct insertion will use the endogenous *H3f3a* promoter to drive expression of GFP reporter, and the first PolyA (PA) will stop further expression, creating a null allele (C). *Cre*-mediated recombination, through mating with transgenic *Cre* mice, causes the GFP reporter and first polyA to be excised, and the endogenous *H3f3a* promoter will drive expression of mutant histone H3.3 cDNA (D).

Fluorescence screening

G1 pups born from G0 CRISPR/Cas9 founders were screened using GFP fluorescent goggles before the thickening of their fur (Figure 2.3 left image). Alternatively, GFP fluorescence screening of tail clippings from two-week-old pups was done through excitation filter "BP 470/40" on a *Leica Upright DMI6000 B* microscope (Figure 2.3 right image).

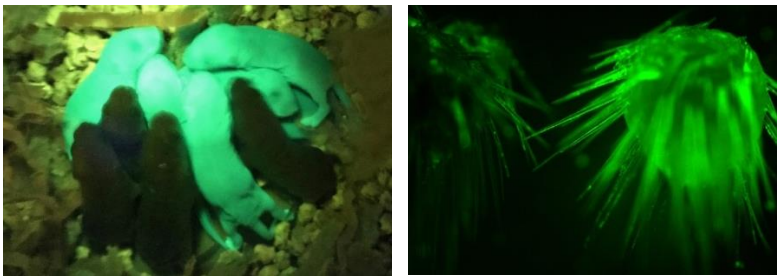

Figure 2.3: GFP Screening of pups and tail clippings. GFP screening was done using GFP fluorescent goggles of live H3.3-G34R P7 G1 mice (on left) and tail clippings through fluorescence microscopy (on right).

Tail lysis

Mouse tail clips were placed in microtubes and 75ul of lysis buffer (25mM NaOH / 0.2 mM EDTA) was added to the microtubes, making sure to submerge tails, then incubated for 30 minutes. Samples were then placed on ice until they cooled. Once samples were cooled, 75ul of neutralization buffer (40 mM Tris HCl, pH 5.5) was added, followed by 300ul of distilled water. The sample was then vortexed and ready for use.

Designing primers to be used for genotyping.

Primer3 was used to design multiple primer pairs flanking various regions of the construct to attempt to confirm correct locus insertion and be used for Sanger sequencing validation (Table 2.5).

Table 2.5: Various primers synthesized for Sanger sequencing validation

Primer Name	**Sequence 5' to 3'**	**Region of Alignment**
cDNAIntron1 Forward	GAACGTGCTTAAGGGGATCA	Outside 5' Homology arm
cDNAIntron1 Reverse	GAAAGGTCGAGTCAAATTACAGC	Outside of 3' Homology arm

cDNAIntron1 Forward-2	CCTCTTTCTTCGGTGAAATCC	Outside 5’ Homology arm
cDNAIntron1 Reverse-2	GGACTACTGCGCCCTACAGA	Outside LoxP 1
cDNAIntron1 Forward-3	GGCTCCTCTTTCTTCGGTGA	Outside 5’ Homology arm
cDNAIntron1 Reverse-3	TCATCAAGGAAACCCTGGAC	Outside LoxP 1
Sequencing-3-F	GGGCCGGGCGGCCGGTGTCG	Outside cDNA
Sequencing-Mutation-F	TTTCCAGATTTGGGGG	Outside cDNA
LongAmpFwd-1	CAGAAATGGAGATGGGGAGCGAGTTTGCCTTCCGCGGG	Outside 5’ Homology arm
LongAmpRev-1	CCCCCCACCATGGCTTTCGATCCAATTCATTTAATTAA	Outside of 3’ Homology arm
LongAmpFwd-2	GCTCCGCTCGCCGTCGGCCTCGTAGGGGCCCACGGAGG	Outside 5’ Homology arm
LongAmpRev-2	AACCAGAGAGACGCCCCCCACCATGGCTTTCGATCCAA	Outside of 3’ Homology arm
LongAmpFwd-3	GGTCTCTCCGTCTCAGCCCAGCAGTGGCACCGCCGCGG	Outside 5’ Homology arm
LongAmpRev-3	CCCCCCACCATGGCTTTCGATCCAATTCATTTAATTAA	Outside of 3’ Homology arm
Long-Amp-PCR-Flex-F-1	CAGAAATGGAGATGGGGAGCGAGTTTGCCTTCCGCGGG	Outside 5’ Homology arm
Long-Amp-PCR-Flex-R-1	CCCCCCACCATGGCTTTCGATCCAATTCATTTAATTAA	Outside of 3’ Homology arm
Long-Amp-PCR-Flex-F-2	GCTCCGCTCGCCGTCGGCCTCGTAGGGGCCCACGGAGG	Outside 5’ Homology arm

Long-Amp-PCR-Flex-R-2	AACCAGAGAGACGCCCCCCACCATGGCTTTCGATCCAA	Outside of 3’ Homology arm
Long-Amp-PCR-Flex-F-3	GGTCTCTCCGTCTCAGCCCAGCAGTGGCACCGCCGCGG	Outside 5’ Homology arm
Long-Amp-PCR-Flex-R-3	CCCCCCACCATGGCTTTCGATCCAATTCATTTAATTAA	Outside of 3’ Homology arm
5-EXT-GFP-F1	CGCGAGCCTCTTAACTGC	Outside 5’ Homology arm
5-EXT-GFP-R1	GTTTACGTCGCCGTCCAG	Flanking GFP
5-EXT-GFP-F2	GCGCGAGCCTCTTAACTG	Outside 5’ Homology arm
5-EXT-GFP-R2	GTTTACGTCGCCGTCCAG	Flanking GFP
5-EXT-GFP-F3	GACCCCAGACCTTCACCAT	Outside 5’ Homology arm
5-EXT-GFP-R3	AACAGCTCCTCGCCCTTG	Flanking GFP
5-EXT-GFP-R4	TCCAGCTCGACCAGGATG	Flanking GFP
Vector 3F1	GGGAGGATTGGGAAGACAAT	Upstream LoxP 2
Vector 3R1	CGAAGCCACAAACACAGAAA	Outside 3’ Homology Arm
Vector 3R2	ACGAAGCCACAAACACAGAA	Outside 3’ Homology Arm
Vector 3R3	AACGAAGCCACAAACACAGA	Outside 3’ Homology Arm
Vector 3R4	GAA CGA AGC CAC AAA CAC AG	Outside 3’ Homology Arm
Vector 3R5	AAT GAA CGA AGC CAC AAA CA	Outside 3’ Homology Arm
3F1	AGA AGCGCGATCACAT GGT	Flanking GFP

3R1	TGGCTGTAATTTGACTCGACCTT	Outside 3' Homology Arm
3F2	CGATCACATGGTCCTGCTGGAGTTCG	Flanking GFP
3R2	TGTTTGTGGCTTCGTTCATTTGA	Outside 3' Homology Arm
3F3	AACGAGA AGCGCGATCACAT	Flanking GFP
3R3	CTGTGTTTGTGGCTTCGTTCAT	Outside 3' Homology Arm
3F4	GAGAAGCGCGATCACATGGT	Flanking GFP
3R4	TGTGTTTGTGGCTTCGTTCATT	Outside 3' Homology Arm

PCR protocol

Primer mix was prepared using the guidelines provided by the *Bioline MyTaq Red Mix* (Cat. No: BIO-25043) protocol (Table 3.1) and modifications to the standard PCR cycling conditions provided by *Bioline MyTaq Red Mix* was used for PCR protocol troubleshooting (Table 2.6, 2.7).

Table 2.6: Standard MyTaq Red Mix PCR reaction set-up

Reagent	**Volume (ul)**
Template DNA (~100ng/ul)	1
MyTaq Mix, 2x	7.5
Forward Primer (10ng/ul)	1
Reverse Primer (10ng/ul)	1
Water (ddH_2O)	4.5

Table 2.7: Standard Bioline MyTaq Red Mix PCR cycling conditions

Temperature	Time
95^oC	1m

95ºC	**15s**	**X 25-35 cycles**
User determined	**15s**	
72ºC	**10s**	

Gel extraction

Bands of interest were cut with a carbon steel single edge razor blade and the DNA was extracted by following the *QIAquick Gel Extraction Kit* (Catalog No. 28115) protocol. In the final extraction step, DNA was resuspended in 30ul of TE Buffer.

Cloning, bacterial transformation, and miniprep

Gel extracted DNA was verified following the procedures of cloning, bacterial transformation, liquid culture and miniprep, as previously described in AIM I.

AIM II, OBJECTIVE II

Sanger sequencing for mouse validation

8ul of miniprep DNA and the common sequencing primers, M13F and M13R, were used to sequence the plasmid, as they are present on the pCRTM2.1-TOPO® vector. In addition, the synthesized reverse primer, cDNAseq4 (5'-CAACGAGCGGATCCAGAC -3'), was sent to Genome Quebec for Sanger sequencing, to ensure sequence coverage of cDNA.

AIM III

Timed matings and embryo collection

All procedures and experiments were performed according to the guidelines of the Canadian Council on Animal Care and approved by the Animal Care Committee of the Montreal Children's Hospital. *Wnt1-Cre2* transgenic mice of C57BL/6 x C3H background were purchased from Jackon`s laboratory (Stock #022137) and mated *H3f3a*$^{LoxP/+}$ mice to induce expression of H3.3-G34R in pre-migratory neural crest cells at E8.5 (mechanism shown in Figure 2.2) and their descendants. Embryonic age was determined by the day of presence of a vaginal plug in females, following the day after mating with a male. If a plug was present, that day was considered embryonic day 0.5 (E0.5).

Dissections and embryo collection

Pregnant female mice were euthanized, and their uteruses were removed and placed in 1x PBS solution. Uteruses were kept in 1x PBS while deciduas were dissected to remove embryos from yolk sacs. Yolk sacs of embryos were collected during dissection and used for genotyping through previously described DNA tail lysis protocol. All E14.5 and E17.5 embryos were weighed upon removal from yolk sacs prior to Alcian Blue and Alizarin Red staining, respectively.

Genotyping Notation

For the purposes of simplicity, the following abbreviations will be used to refer to the genotypes of embryos as follows (Table 2.8): Wildtype (*H3f3a*$^{+/+}$) and *Wnt1-Cre2* transgene (tg) carrying (*H3f3a*$^{+/+}$; *Wnt1-Cre2 tg*) embryos were denoted as controls **CTRL**, heterozygous (*H3f3a*$^{LoxP/+}$) are **HEMI H3.3A** because they have one non-functional *H3f3a* allele, homozygous mutants (*H3f3a*$^{LoxP/LoxP}$) are denoted **H3.3A NULL** because they have two non-functional *H3f3a* alleles**,** and mutant embryos expressing H3.3-G34R in NCC (*H3f3a*$^{LoxP/+}$*; Wnt1-Cre2 tg)* are **HET G34R NCC**. In some cases, the *Wnt1-Cre2* transgene is expressed in the germline of mice early in development. If these mice are also *H3f3a*$^{LoxP/+}$ or HEMI H3.3A, they may have recombined mutant H3.3-G34R alleles in their germline, and furthermore, have the potential to give rise to offspring that are constitutive for the H3.3-G34R mutation. The endoderm/mesoderm derived yolk sacs of embryos were collected for genotyping, if those samples showed presence of the H3.3-G34R recombined band (explained in Figure 3.2), this suggests that these embryos express mutant H3.3-G34R in cells outside of the neural crest cell lineage, are present in all germ layers, and therefore constitutive heterozygous for H3.3-G34R. To distinguish constitutive heterozygous embryos from neural crest cell only mutants, heterozygous embryos (*H3f3a*$^{G34R/+}$) are denoted as **HET G34R.** Lastly, constitutive homozygous embryos expressing H3.3-G34R in every cell (*H3f3a*$^{G34R/G34R}$) are denoted as **HOMO G34R**. Genotypes and their abbreviations are summarized below (Table 2.8)

Table 2.8: Genotypes of generated mice and their abbreviations

Standard Nomenclature	**Abbreviation**
H3f3a$^{+/+}$	**CTRL**
H3f3a$^{+/+}$*; Wnt1-Cre2 tg*	**CTRL**
H3f3a$^{LoxP/+}$	**HEMI H3.3A**
H3f3a$^{LoxP/+}$*; Wnt1-Cre2 tg*	**HET G34R NCC**

H3f3a$^{LoxP/LoxP}$	**H3.3A NULL**
H3f3a$^{G34R/+}$	**HET G34R**
H3f3a$^{G34R/G34R}$	**HOMO G34R**

Cartilage preparations – Alcian Blue Staining

Upon removal from yolk sac, E14.5 embryos were placed in small glass scintillation vials and fixed in Bouin's solution for two hours. Embryos were then washed eight times in a 70% ethanol + 0.1% NH4OH solution over 24 hours, followed by two equilibration washes with 5% acetic acid (one hour each). Embryos were then stained in a 0.05% Alcian blue 8GX (Fisher) in 5% acetic acid solution for two hours. Samples were then rinsed twice with 5% acetic acid for one hour each and washed twice with methanol for one hour each. Finally, embryos were cleared through placement in a final solution of BABB (benzyl alcohol: benzyl benzoate, 1:2) and visualized under light microscope (Leica MZ6 Infinity1 stereomicroscope) for analysis. This protocol was performed as described by Jegalian & Robertis, 1992 (Jegalian & De Robertis, 1992).

Skeletal preparations – Alcian Blue and Alizarin Red Staining

A modified protocol (Rigueur and Lyons, 2014) was used to analyze both bone and cartilage in E17.5 embryos. Upon removal from yolk sac, embryos were skinned and eviscerated using forceps. Embryos were then placed in a small glass scintillation vial and fixed in 100% ethanol for 24 hours at room temperature on a rocker. Next, embryos were placed in 100% acetone on a rocker at room temperature for 24 hours and then submerged in an Alcian Blue/Alizarin Red stain solution composed of a 1:1:1:17 ratio of 0.3% Alcian Blue (Sigma 8GX), 0.1% Alizarin Red (Sigma), Glacial acetic acid (*Fisher Scientific*) and 70% ethanol, respectively. Embryos were kept in the stain for 3-4 days at 37^{o}C on a rocker. Samples were then rinsed in distilled water and cleared in 1% KOH at room temperature overnight. Lastly, samples were placed in a final solution of 50% glycerol/1% KOH and once fully cleared, were visualized by light microscope (Leica MZ6 Infinity1 stereomicroscope).

Image analysis

Cartilage and skeletal preparations were assessed through blind analysis. Embryos were observed under a *Leica MZ6 Infinity1* stereomicroscope for visible defects in cartilage and bone of the cranial base. Embryos were assessed for misshapen or missing cartilages or bone through absence or reduction of Alcian Blue and Alizarin Red staining, respectively.

Genotyping of embryos

H3f3a genotyping primers, 5-EXT-GFP-F1 (CGCGAGCCTCTTAACTGC), 5-EXT-GFP-R1 (GTTTACGTCGCCGTCCAG) and G34R reverse mutagenesis primer (ATGAGGTTTCTT CACCC**T**TCCAGTAGAGGGCGC (Table 2.5, 2.1) were used to genotype mice using PCR conditions previously described (Table 2.6). *Wnt1-Cre2* mouse genotyping was performed using the protocol provided on the Jackson`s laboratory website (Protocol #25394: Standard PCR Assay).

The following chapter will describe the results for aims I, II, and III.

CHAPTER III: RESULTS

AIM I

Quick-change mutagenesis was performed for all H3.3 plasmids

The G34R, G34V and wildtype templates were generated first because the mutation site was in the same location. The wildtype repair template was then used as the backbone to generate the K36M and K27M repair templates. Therefore, each repair template differed by a single base substitution in their cDNA and targeted the same locus for eventual use in CRISPR/Cas9 mediated integration.

Successfully mutated clones were synthesized for all H3.3 plasmids

Ten colonies were picked for the G34R, G34V, and WT plasmid containing plates to screen for successful mutagenesis. The K36M and K27M plates contained less than ten colonies, with 7 colonies screened for K36M and six colonies screened for K27M. There were 5/10 successfully mutated G34R clones, 2/10 G34V, 4/10 wildtype, 5/7 K36M and 2/6 K27M (Table: 3.1)

Table 3.1: Number of plasmid clones picked and successfully mutated for each H3.3 mutation

Plasmid	**# of clones picked and sent for sequencing**	**# of successfully mutated clones**
G34R	10	5
G34V	10	2
WT	10	4
K36M	7	5
K27M	6	2

All H3.3 plasmids were successfully generated

One successfully mutated clone for each H3.3 mutation was chosen to use in a maxiprep for large scale preparation and again verified through Sanger sequencing. All plasmids were successfully synthesized through quick change mutagenesis (Table 3.2).

Table 3.2: Plasmids synthesized through quick change mutagenesis

Plasmid Repair Template	Associated Cancer	Status
G34R	Pediatric Glioblastoma	Generated
G34V	Pediatric Glioblastoma	Generated
Wildtype (G34)	-	Generated
K36M	Chondroblastoma	Generated
K27M	D.I.P.G	Generated

AIM II

PCR primers and conditions were successfully identified to validate mutant mice

PCR cycling conditions were identified to allow for genotyping of mutant mice (Table 2.10). For reaction mix, reagent volumes from the previously described *MyTaq Red Mix* guideline (Table 3.3) were used.

Table 3.3: Synthesized PCR program used to genotype mice

Temperature	Time	
95^{o}C	1m	
95^{o}C	30s	X 33 cycles
62.5^{o}C	1m	
72^{o}C	1m 44s	
72^{o}C	10m	
4^{o}C	hold	

PCR that successfully amplified the entire 3kb modified locus could not be identified. Therefore, primer pairs amplifying shorter regions of the construct were used. Two primer pairs (5-EXT-GFP-F1, 5-EXT-GFP-R1 and 3F4, 3R4) were designed to amplify sequences in *H3f3a*

intron 1 that were 5' and 3' to sequences used in the targeting construct (Fig 3.1A). Primers, 5-EXT-GFP-F1 and 5-EXT-GFP-R1, were used to amplify a 700 bp product which contained the 5' LoxP sequence and splice acceptor (Figure 3.1). Primers 3F4 and 3R4 amplified a 1.74kb product that included the 3' LoxP sequence and mutant cDNA (Figure 2.4A). The two sets of primers used to validate homologous recombination into intron 1 of *H3f3a* were: 5-EXT-GFP-F1: CGCGAGCCTCTTAACTGC, 5-EXT-GFP-R1:GTTTACGTCGCCGTCCAG and 3F4: GAGAAGCGCGATCACATGGT, 3R4: TGTGTTTGTGGCTTCGTTCATT (Table 2.5).

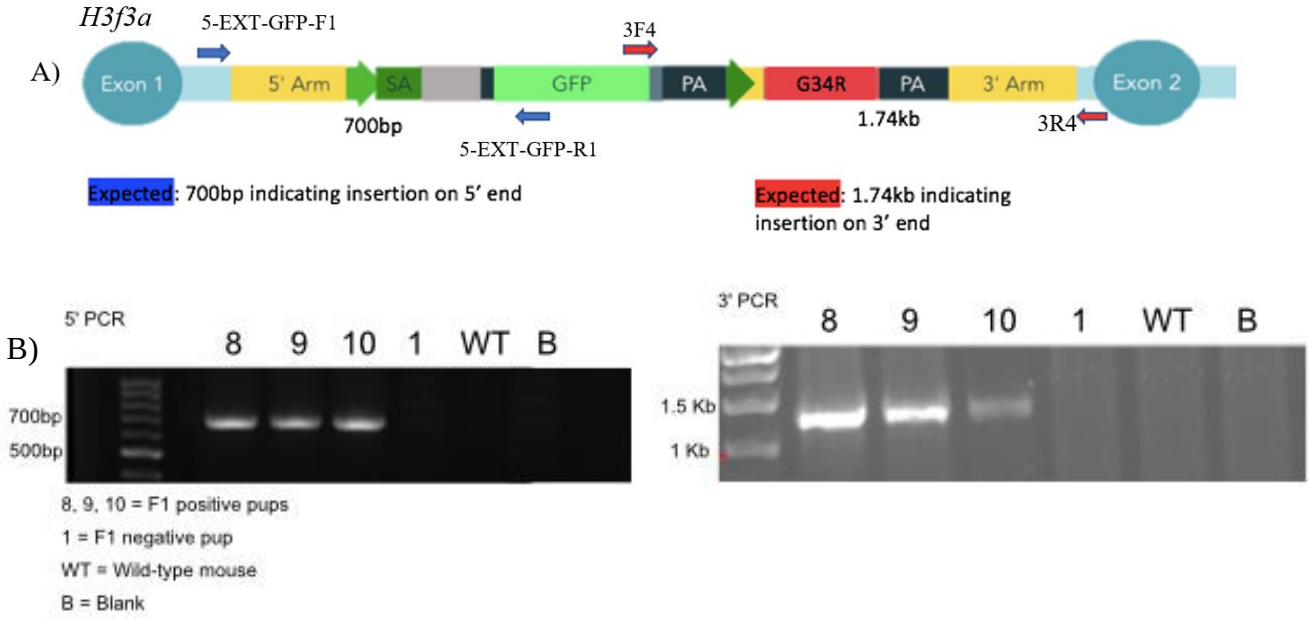

Figure 3.1: Synthesized PCR design used for genotyping mutants. PCR schematic detailing regions of newly generated primers used in screening pups, that validate correct locus insertion of the construct, through external 5' and 3' amplification (A). Primers 5-EXT-GFP-F1 and 5-EXT-GFP-R1 amplify a 700 bp product and primers 3F4 and 3R4 amplify a 1.74 kb product (A). Agarose gel results using primers 5-EXT-GFP-F1, 5-EXT-GFP-R1 (left) and 3F4, 3R4 (right) in G1 positive mice (8, 9, 10), negative mice (1), and wild-type mouse (B).

Mouse lines have been established from 5/6 of the repair templates

Total number of G0 founder mice born for each line are as followed: 53 mice for G34R, 62 for G34W, 36 for WT, 42 for K36M and 80 for K27M. Out of the G0 founders born for G34R, 4/53 founder mice were positive through PCR. Each founder was backcrossed and gave rise to G1 pups that were positive through PCR screening. The 5' and 3' amplicons were

sequenced and validated for correct locus insertion and intact plasmid components. All four G1 pups had the targeted insertion. For G34W, 9/62 founders were positive. When mated, only 2 founders were capable of germline transmission, G1 pups were screened and both were validated. For the wildtype line, 1/36 founders were positive and gave rise to G1 positive pups that were validated for correct insertion. For K36M, 4/42 founder mice were positive and 2/4 were able to give rise to positive G1 mice that were sequence confirmed. Finally, 1/80 K27M founders were positive and this single founder gave rise to G1 pups with correct insertion. CRISPR/Cas9 efficiencies for each line are listed below (Table 3.4).

Table 3.4: Number of founders and F1 pups generated for each H3.3 mutant line

H3.3-Repair Template	# of G0 founders born	# of founders positive for both target bands	# of founders able to transmit mutation and produced sequence verified G1 offspring	# of G1 pups sequenced and used to establish line	CRISPR/Cas9 knock in efficiency
G34R	53	4	4	4	7.5%
G34W	62	9	2	2	3.2%
WT	36	1	1	2	2.7%
K36M	42	4	2	2	4.8%
K27M	80	1	1	2	1.3%

Mouse lines were created for G34R, Wildtype, K36M, G34W, and K27M H3.3 mutations. Plans for G34V mouse line generation were postponed, given it is a less frequently occurring mutation in paediatric glioblastoma compared to G34R (Table 3.5).

Table 3.5: Status of mutant mouse line generation

Mouse Line	**Status**
G34R	Generated
G34V	Not Generated (Postponed)

Wildtype (G34)	Generated
K36M	Generated
K27M	Generated
G34W	Generated

Colonies generated adhered to Mendelian segregation

H3f3a$^{LoxP/+}$ mice were mated to wildtype mice to establish our colony and assess viability of heterozygous, *H3f3a*$^{LoxP/+}$, mutant mice. Mating's resulted in generation of wild type and heterozygous mice that adhered to Mendelian ratios (Table S1), indicating that heterozygous mice are viable and fertile.

A robust PCR program was designed to genotype mutants

Wnt1-Cre2 transgenic mice express *Cre* in pre-migratory neural crest cells at E8.5 and were mated to *H3f3a*$^{LoxP/+}$ mice to express H3.3-G34R in neural crest cells (mechanism shown in Figure 2.2). Evidence of germline recombination in *Wnt1-Cre2* transgenic mice causing generation of constitutive mutant mice has been reported (The Jackson Laboratory, jax.org/strain/022137), leading to the design of a 3-primer PCR using 5-EXT-GFP-F1 (CGCGAGCCTCTTAACTGC), 5-EXT-GFP-R1 (GTTTACGTCGCCGTCCAG) and the G34R reverse mutagenesis primer (ATGAGGTTTCTT CACCC**T**TCCAGTAGAGGGCGC). PCR was optimized to amplify **CTRL** (or wild type) (1.3kb), **HEMI H3.3A** (LoxP flanked) (700bp) and recombined mutant cDNA (**G34R**) (800bp) amplicons (Figure 3.2)

A

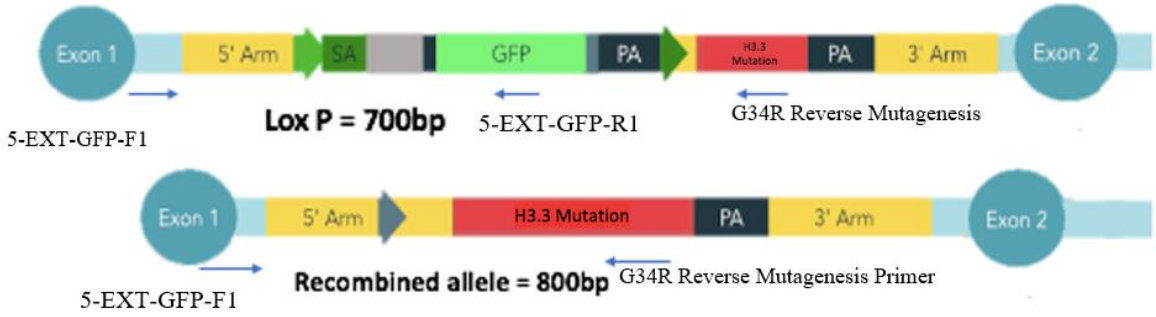

B

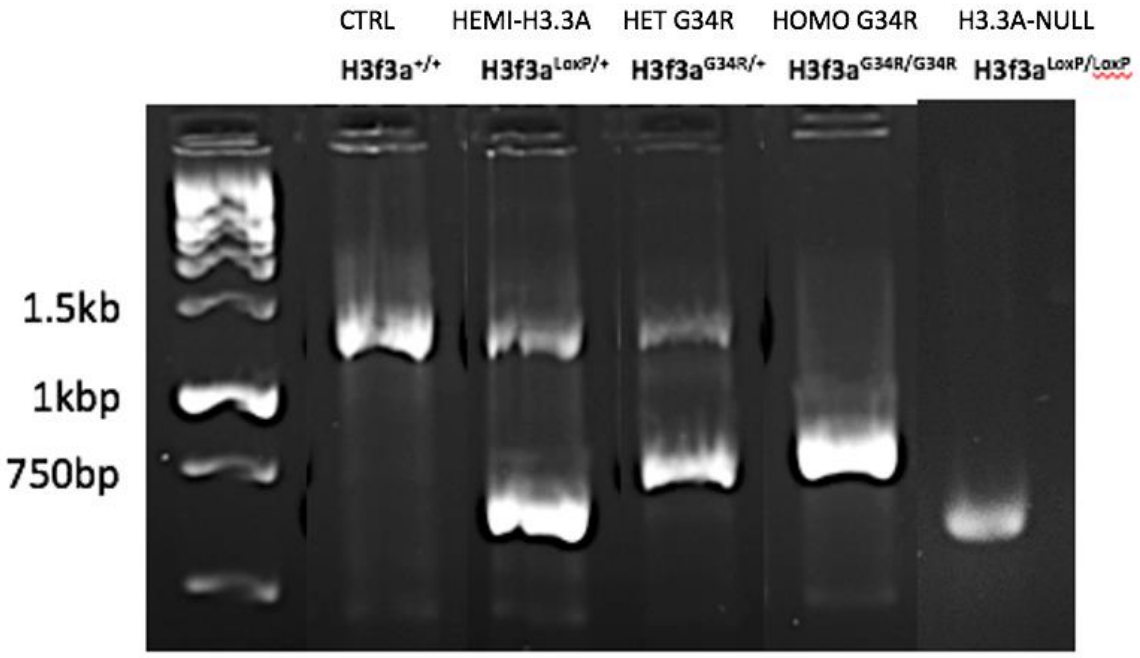

Figure 3.2: New 3-primer PCR used to genotype mutant mice. Primers 5-EXT-GFP-F1, 5-EXT-GFP-R1 and the G34R reverse mutagenesis primer flanking cDNA was used in PCR genotyping of mutants. PCR was optimized to amplify wild-type (1.3kb), LoxP flanked (700bp) and mutant cDNA (G34R) (800bp) amplicons (A). PCR results on agarose gel showing expected amplicon sizes for CTRL, HEMI-H3.3A, HET G34R, HOMO G34R and H3.3A-NULL embryo genotypes (B).

AIM III

ANOVA of E14.5 and E17.5 embryo weight was statistically significant.

Six litters of E14.5 staged embryos (N=36) and six litters of E17.5 staged embryos (N=57) were weighed upon removal from the yolk sac (Table S2). Genotypes with at least five embryos were analyzed for differences in weight by ANOVA, followed by a Tukey HSD test to compare the mean weight of all possible genotypic pairs to clarify where the significant differences between genotypic groups lied. Weight analysis for both E14.5 (Table S4) and E17.5 (Table S5), revealed to be statistically significant, with F-Ratio = 4.098 and p =0.00657** for E14.5 embryos, and F-Ratio = 4.13671 and p = 0.00661** for E17.5 embryos (Table S4, S5).

Tukey HSD revealed that when comparing mutants to controls, only E17.5 H3.3A-NULL embryos were significantly smaller than control littermates. All other mutant groups when compared to controls were non-significant (Figure 3.3, 3.4, 3.7, 3.9). The following figures, comparing weight averages, will only display comparison of controls and a single mutant genotypic group for simplicity. The p values contained within the figure are derived from the Tukey HSD test (Table S4, S5).

Weight of HEMI-H3.3A and HET G34R NCC embryos not significantly different from controls.

Analysis of weight revealed that HEMI-H3.3A embryos were not significantly different from controls at E14.5 and E17.5 (Figure 3.3). Similarly, weight of HET G34R NCC embryos was not significantly different from controls at E14.5 and E17.5 (Figure 3.4).

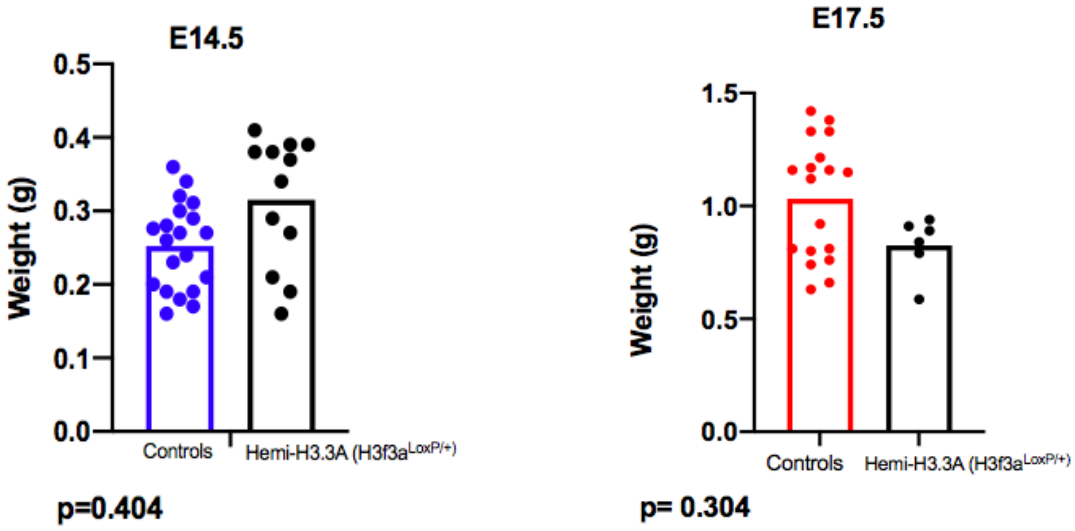

Figure 3.3: Weight averages of E14.5 and E17.5 control vs Hemi-H3.3A mutant embryos. Average weight across all genotypic groups were assessed through ANOVA followed by Tukey HSD. Figure only displays comparison of controls and Hemi-H3.3A embryos for simplicity. P values, from Tukey HSD, showed HEMI-H3.3A E14.5 (N=12) and E17.5 HEMI-H3.3A (N=6) mutants were not significantly different (p=0.404 and p=0.304, respectively) in weight from stage matched E14.5 (N=20) or E17.5 controls (N=18). Data point represents one embryo.

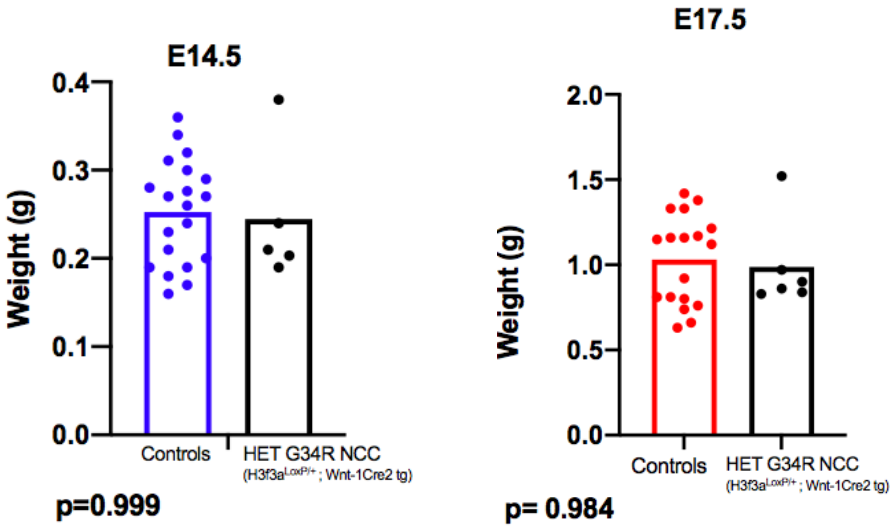

Figure 3.4: Weight averages of E14.5 and E17.5 control vs HET G34R NCC **mutant embryos.** Weight across all genotypic groups were assessed through ANOVA. Figure only displays comparison of controls and HET G34R NCC embryos for simplicity. P values, from Tukey HSD, showed HET G34R NCC E14.5 (N=5) and E17.5 HET G34R NCC (N=6) mutants were not significantly different (p=0.999 and p=0.984, respectively) in weight from stage matched controls (E14.5 (N=20) E17.5 (N=18)). Data point represents one embryo.

Craniofacial elements of HEMI-H3.3A and HET G34R NCC embryos not significantly different from controls.

E14.5 and E17.5 cartilaginous and bony elements of the cranial vault and base of HEMI-H3.3A and HET G34R NCC embryos were comparable to those of their control litter mates, evidenced through Alcian Blue and Alizarin Red staining (Figure 3.5, 3.6).

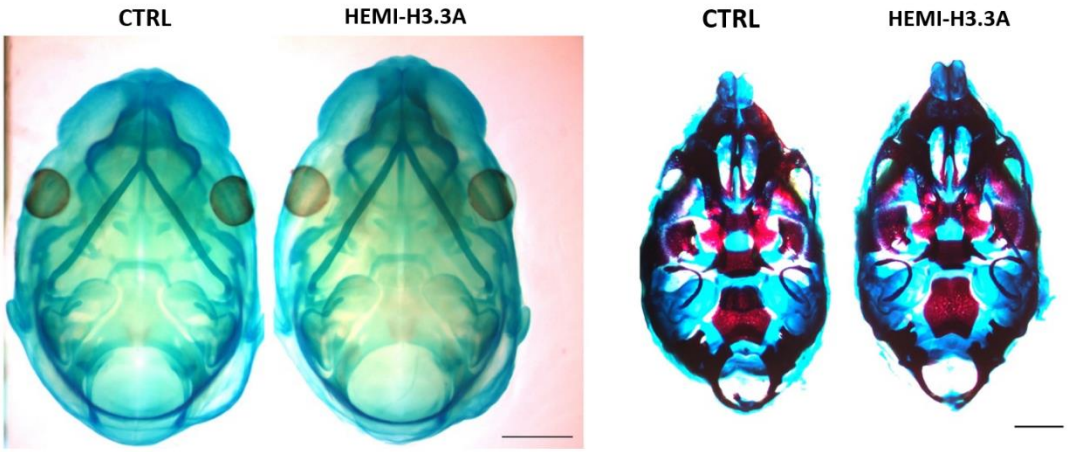

Figure 3.5: Comparison of craniofacial elements of HEMI-H3.3A and control embryos. No phenotypic differences seen in head cartilages or bones of E14.5 (left) or E17.5 (right) control embryos and HEMI-H3.3A mutants. Scale bars =1mm.

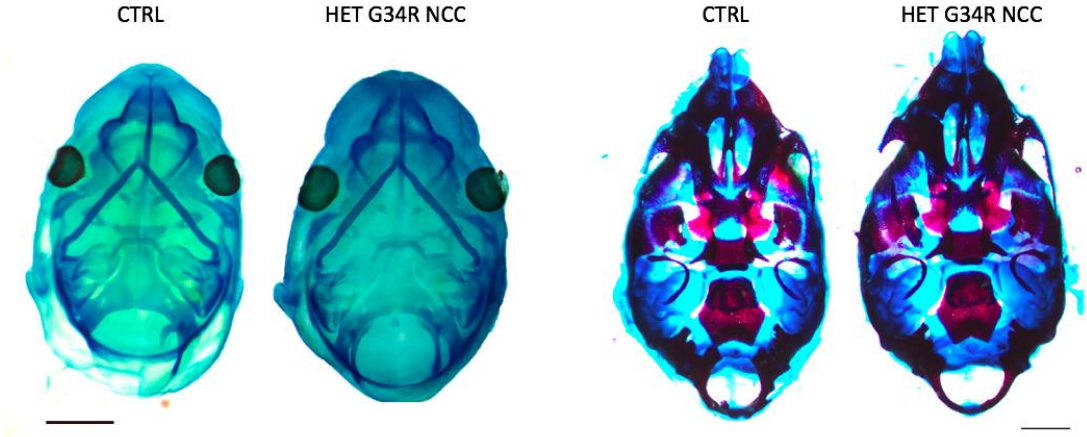

Figure 3.6: Comparison of craniofacial elements of HET G34R NCC and control embryos. No phenotypic differences were seen in the head cartilages or bones of E14.5 (left) or E17.5 (right) controls and HET G34R NCC mutants. Scale bars =1mm

Weight of constitutive E14.5 HET G34R, E14.5 HOMO G34R, and E17.5 HET G34R mutants were not significantly different from controls.

E14.5 HET G34R (N=7) and HOMO G34R (N=5) mutants were not significantly different in weight from controls with p = 0.0406 and p= 0.981, respectively. E17.5 HET G34R embryo weight (N=10) also did not significantly differ from controls with p=0.999 (Figure 3.7).

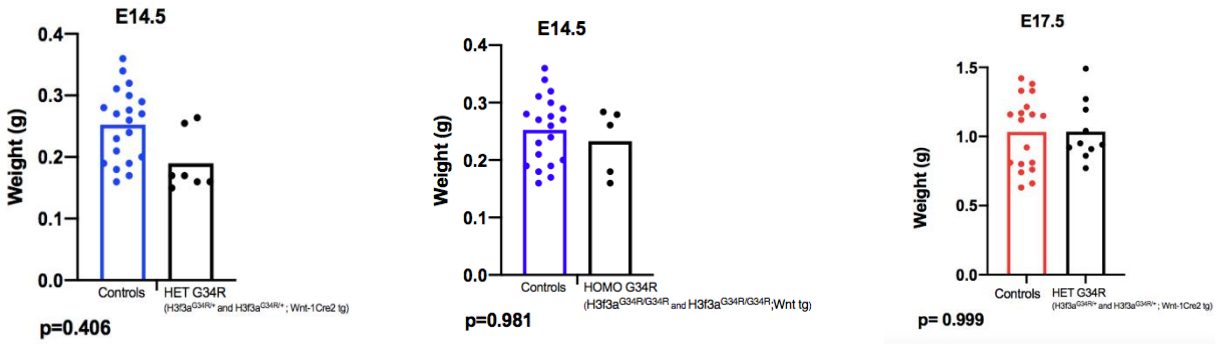

Figure 3.7: Weight averages of control vs HET G34R and HOMO G34R mutant embryos. Weights across all genotypic groups were assessed through ANOVA. Figure only displays the comparison of two genotypic groups for simplicity. P values, derived from Tukey HSD analysis, show both E14.5 HET G34R (N=20) and HOMO G34R (N=5) mutants were not significantly different (p=0.406 and p=0.981, respectively) in weight from controls (N=20) and E17.5 HET G3R embryos (N=10) also did not significantly differ (p=0.999) from controls (N=18). Data point represents one embryo.

Craniofacial elements of constitutive HET G34R and HOMO G34R embryos were hypoplastic compared to controls.

E14.5 and E17.5 HET G34R and HOMO G34R mutants showed hypoplasia of neural crest cell derived cartilage and bone compared to controls. Cartilage derivatives of the head showed reduced Alcian blue staining in both HET G34R and HOMO G34R embryos. At E14.5, all HET G34R mutants (7/7) and majority of HOMO G34R mutants (3/5) showed absence of Alcian Blue staining in the ala temporalis, basitrabecular process, hypophyseal, parachondral and canicular region of the auditory capsule cartilages compared to control embryos (Figure 3.8). At E17.5, HET G34R (5/10) and HOMO G34R (1/3) had similar defects with visible bone hypoplasia, seen through reduction in Alizarin Red staining. Hypoplastic bones included the squamous, sphenoid, basosphenoid, tympanic ring, and zygomatic arch (Figure 3.8).

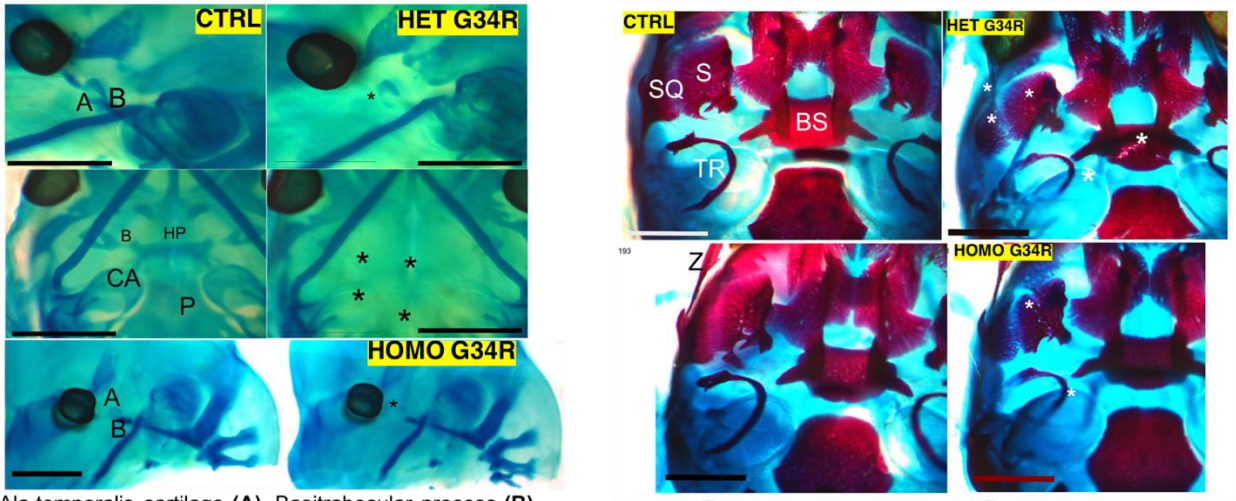

Ala temporalis cartilage **(A)**, Basitrabecular process **(B)**, Hypophyseal cartilage **(HP)** Parachondral cartilage **(P)**, Canicular region of the auditory capsule **(CA)**

Squamous **(SQ)**, Sphenoid **(S)**, Basosphenoid **(BS),** Tympanic Ring **(TR),** Zygomatic Arch **(Z)**

Figure 3.8: Comparison of craniofacial elements of HET G34R, HOMO G34R and control embryos. E14.5 and E17.5 HET G34R and HOMO G34R embryos show hypoplasia of neural crest cell derived cartilages and bone, respectively. Image panel on left shows E14.5 controls vs mutant embryo heads. HET G34R (7/7) mutants and HOMO G34R (3/5) mutants showed reduction in the ala temporalis, basitrabecular process, hypophyseal, parachondral, and canicular region of the auditory capsule cartilages compared to control embryos. Image panel on the right show E17.5 controls vs HET and HOMO G34R mutant embryo heads. E17.5 HET G34R (5/10) and HOMO G34R (1/3) showed reduction in the squamous, sphenoid, basosphenoid, tympanic ring, and zygomatic arch bones. Scale bars =1mm.

E17.5 H3.3A NULL embryos were significantly smaller than control littermates and embryos showed severe bone and cartilage hypoplasia.

Tukey HSD identified that E17.5 H3.3A-NULL embryos (N=7) were significantly smaller than controls (N=18) with p= 0.02* (Figure 3.9). E17.5 H3.3A-NULL embryos showed severe bone hypoplasia compared to controls. Embryos had ossification defects in bones also affected in constitutive HET G34R mutants. Alizarin red staining was reduced in the squamous, sphenoid, basosphenoid, basioccipital, tympanic ring, zygomatic arch, palatine, and palatal process of the palatine bones (Figure 3.10).

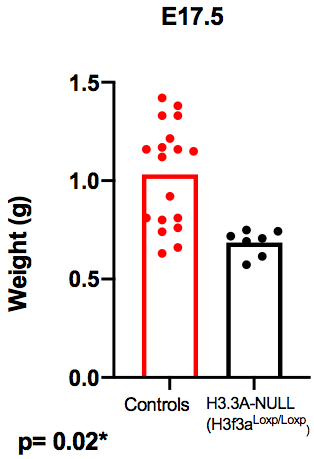

Figure 3.9: Weight average of E17.5 control and H3.3A-NULL embryos. Weights across all genotypic groups were assessed through ANOVA. Figure only displays the comparison of controls and H3.3A-NULL embryos for simplicity. P values, derived from Tukey HSD analysis, show H3.3A-NULL embryos were significantly smaller than control littermates (p=0.02*). Data point represents one embryo.

Squamous **(SQ)**, Sphenoid **(S)**, Basosphenoid **(BS)**, Basioccipital bone **(BO)**, Tympanic Ring **(TR)**, Zygomatic Arch **(Z)**, palatine **(PL)**, palatal process of the palatine **(PPPL)**

Figure 3.10: E17.5 H3.3A-NULL embryos showed severe hypoplasia of both cartilage and skeletal elements compared to controls. Image on left shows E17.5 control embryos with labelled head bones. Middle and right images show E17.5 H3.3A-NULL embryos. Yellow stars indicate areas of bone hypoplasia. Hypoplastic bones included: the squamous, sphenoid, basosphenoid, basioccipital, tympanic ring, zygomatic arch, palatine, and palatal process of the palatine bones. Scale bars =1mm.

Z score analysis revealed significant difference in the proportion of affected embryos of HET G34R, HOMO G34R and H3.3A-NULL mutants compared controls.

Mutant genotypes with phenotypic defects, and at least five embryos for comparison, were analyzed through Z-score analysis to determine if the proportion of affected embryos seen was significant from controls. When comparing the proportion of affected E14.5 control embryos (2/12) versus the proportion seen in HET G34R embryos (7/7), Z score analysis revealed a significant difference (p= 0.0004***). The proportion of affected control and HOMO G34R (3/5) embryos however was not significant (p=0.073) (Figure 3.11). When comparing the proportion of affected embryos in E17.5 controls (1/17) versus HET G34R embryos (5/10), there was a significant difference (p= 0.009**) (Figure 3.12). Lastly, the number of affected control and mutant H3.3A-NULL embryos (6/7) was also significant (p=0.00001***) (Figure 3.12).

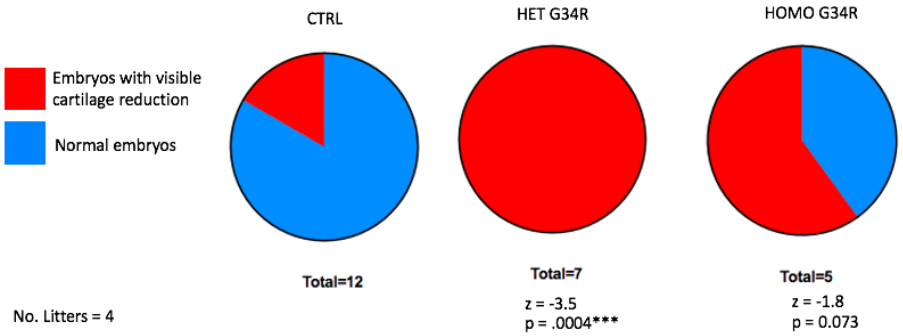

Figure 3.11: Z-score analysis of E14.5 embryo heads with cartilage defects in CTRL, HET G34R and HOMO G34R embryos. Z score analysis assessing significance in the proportion of affected E14.5 embryo heads with cartilage defects compared to controls. Proportion of affected controls (2/12) and HET G34R (7/7) embryos was significant (z=-3.5, p=0.0004***) while proportion of affected controls vs HOMO G34R embryos (3/5) was non-significant (z=-1.8, p= 0.073).

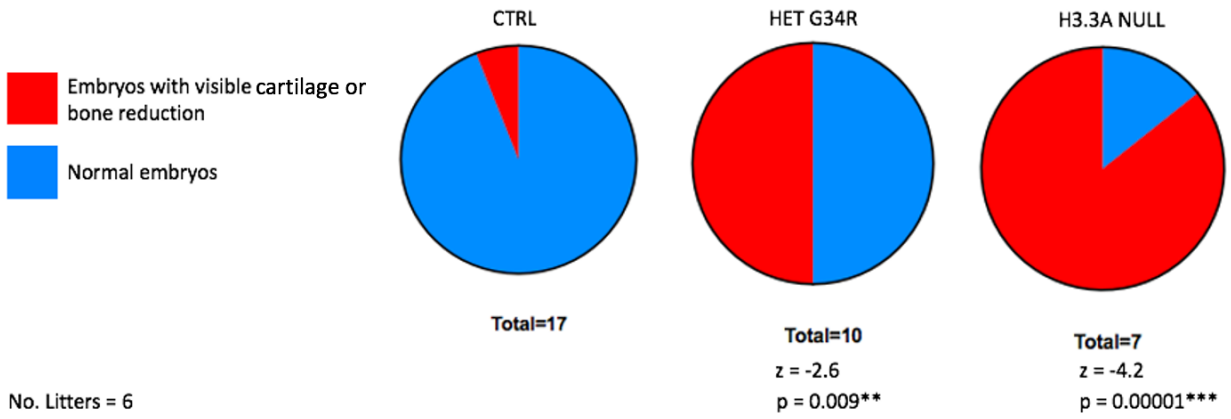

Figure 3.12: Z-score analysis of E17.5 embryo heads with cartilage or bone defects in CTRL, HET G34R and H3.3A-NULL embryos. Z-score analysis assessing significance in the proportion of affected embryo heads with bone or cartilage defects compared to controls. Proportion of affected E17.5 controls (1/17) vs HET G34R (5/10) embryos was significant (z=-2.6, p=0.009**) and proportion of affected controls (1/17) vs H3.3A-NULL (6/7) embryos was also significant (z=-4.2, p= 0.00001***).

E17.5 HET G34R embryos showed ossification defects primarily in neural crest cell derived bones of the skull while H3.3A-NULL embryos showed severe ossification defects in both neural crest cell derived and mesoderm derived head bones.

Interestingly, E17.5 HET G34R embryos showed ossification defects primarily in the NCC-derived bones of the skull, such as the zygomatic arch, squamous, sphenoid and tympanic ring bones (Cibi et al., 2019; Chapman, 2011) H3.3A NULL embryos showed more severe reductions in the same NCC-derived bones in addition to mesoderm-derived bones, such as the basioccipital and exoccipital bone.

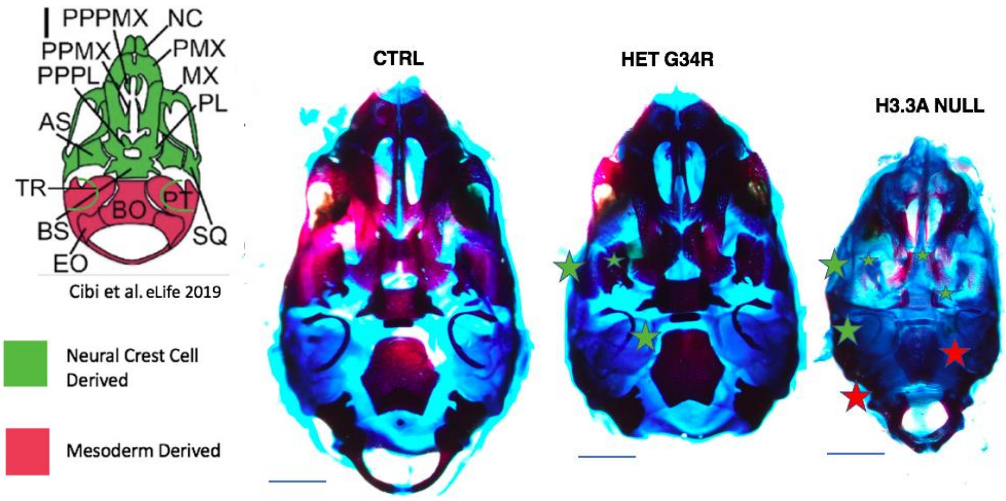

Figure 3.13: HET G34R embryos show reduction in NCC-derived bones while H3.3A NULL embryos show severe reduction in both NCC and mesoderm derived bones. Labelled illustration of E17.5 mouse head (on left) is adopted from (Cibi et al., 2019) and shows regions of neural crest cell derived (green) and mesoderm derived (red) head skeleton. Reduction of neural crest cell derived (green stars) and mesoderm derived (red stars) head bones are shown on the right in our HET-G34R and H3.3A-NULL mutants. HET G34R embryos show reduction in NCC-derived bones while H3.3A NULL embryos show severe reduction in both NCC and mesoderm derived bones. Scale bars =1mm. Abbreviations: premaxilla (PMX), palatal process of premaxilla (PPPMX), palatal process of maxilla (PPMX), palatal process of palatine (PPPL), nasal capsule (NC), maxilla (MX), palatine (PL), sphenoid (AS), tympanic ring (TR), basisphenoid (BS), basioccipital (BO), palatine (PT), squamous (SQ), and exoccipital (EO).

The following chapter is the discussion section, focusing on results obtained in Aim III.

CHAPTER IV: DISCUSSION

Craniofacial elements of E17.5 HEMI- H3.3A embryos showed no difference compared to controls while E17.5 H3.3A NULL embryos showed severe ossification defects.

H3.3 is encoded by the two genes, *H3f3a* and *H3f3b*. Based on previous studies, it is widely accepted that mice hemizygous for *H3f3a* (*H3f3a*$^{+/-}$), are viable and comparable to their wild-type counterparts (Couldrey et al., 1999); indicating that a single *H3f3a* allele is sufficient for mouse development (Couldrey et al., 1999; Tang et al., 2015; Jang et al., 2015). My data is consistent with this finding as HEMI H3.3A mice were indistinguishable from control mice, both postnatally and throughout development. Specifically, E14.5 and E17.5 HEMI-H3.3A embryos were not significantly different in weight or in cartilage and bone formation and differentiation when compared to controls.

Histone H3.3 is ubiquitously expressed throughout development, and though *H3f3a* and *H3f3b* encode the exact same protein, they differ in their patterns of expression (Jang et al. 2015; Couldrey et al., 1999; Bryant et al. 2020). Differences in the expression patterns of the two genes may explain why previous studies have reported different phenotypes in mice depending on whether *H3f3a* or *H3f3b* is knocked out (Tang et al., 2015; Bush et al., 2013). While mice hemizygous for *H3f3a* are fertile, hemizygosity of *H3f3b* in mice has been reported to result in male sterility (Tang et al., 2015), suggesting that *H3f3b* may be more important in mice fertility. Mixed results have been found regarding the effects of *H3f3a* gene knockout and knockdown in mice. While knockout *H3f3a* mice, generated through homozygous deletion of exon 2 through a gene-trap targeting intron 1, were viable (Jang et al., 2015), mice homozygous for a H3.3A gene trap allele showed reduced viability (Couldrey et al., 1999). In this model, mice were generated using a similar as ours, through insertion of a gene trap vector into intron 1, inhibiting expression of the endogenous exons *H3f3a*. In this study, mutants at P0 (the day of birth) could not be distinguished from control littermates, however, within the first 24 hours 50% of mutants died. Remaining mutants were significantly smaller than controls and this persisted even at four months of age (Couldrey et al., 1999). Reduced size in males was also found in a study which used a targeted *H3f3a* allele. Male *H3f3a* knockout mice (*H3f3a*$^{-/-}$) were significantly smaller than their wildtype counterparts at the post-natal age of three and six weeks (Tang et al. 2013, 2015). Females also exhibited a similar trend that suggested growth deficiency, however the difference was not significant. Our data supports a growth deficiency in H3.3A-NULL embryos, as they were significantly smaller in weight than controls. In addition, we show the removal of

H3.3A protein is detrimental to formation of head bones, however, the viability of our knockout *H3f3a* mice was not adequately assessed in this study. Only one mating pair was set up and two litters were born totaling 13 pups. No H3.3A-Null (*H3f3a*$^{LoxP/LoxP}$) mice were born, 10/13 were *H3f3a*$^{LoxP/+}$ (HEMI H3.3) and 3/10 were wildtype and Chi square analysis was non-significant (p= 0.076). More litters must be produced from multiple breeding pairs in order to properly assess the viability of H3.3A-NULL embryos; enabling us to deduce if this severe reduction in cartilaginous structures and bone ossification contributes to lethality. Furthermore, our knockout mouse embryos were generated using a C57BL/6; C3H mixed background. This differs from previously generated mice, which used inbred mouse strains (Couldrey et al., 1999; Tang et al., 2015; Bush et al., 2013; Tang et al., 2013), with one study (Jang et al., 2015) using an alternative mixed genetic background (C57BL/6;129). Differences in genetic background mean the direct comparison of models should be made cautiously, as the interaction between genes, environment, and genetic background can dictate phenotypic severity or manifestation of a mutation.

Off-target effects are unlikely to contribute to the phenotypes seen. Mice used for analysis were derived from G3 and G4 mice mated to wildtype mice or each other (familial mating); meaning they were either three or four backcrosses from the CRISPR. However, it is possible that embryos generated from familial mating potentially have amplification of off-target effects through allele fixation; additional backcrossing (to G10) and cartilage/bone analyses is needed to rule this out.

Skeletal defects of H3.3-A-NULL embryos were similar to phenotypes seen in an aforementioned zebrafish model with dominant-negative mutation in H3.3 (Cox et al., 2012). In that study, a dominant-negative point mutation (D123N) in *h3f3a* caused an inability of zebrafish mutants to form neural crest-cell derived bone and this was attributed to an under enrichment of H3.3 in nucleosomes. It was shown that D123N mutant h3.3, not only was not incorporated into nucleosomes, but in addition, inhibited wildtype h3.3 from being incorporated into nucleosomes. The mutant D123N protein had an affinity for wildtype h3.3 and formed aberrant protein complexes leading to h3.3 depletion in nucleosomes. Removal of H3.3A protein in our mouse mutants could similarly decrease H3.3 incorporation into nucleosomes, resulting in a similar phenotype of a reduction or absence of cartilaginous structures, and decrease in skeletal ossification. This study is limited in drawing conclusions on the level of H3.3 protein present in

mutants, as western blot analysis must be done to quantify H3.3 protein levels. An additional experiment that could help shed light on the mechanisms behind this severe phenotype is H&E staining to assess potential defects in cellular morphology.

H3.3 depletion was previously reported to cause mitotic abnormalities in cells, such as formation of anaphase bridges and lagging chromosomes, leading to insurmountable DNA damage and subsequent p53-mediated apoptosis (Jang et al., 2015). Severe reduction of bone and cartilage elements in our E17.5 H3.3A-NULL embryos suggests there is reduced cell proliferation or cell death. This could explain why E17.5 H3.3A-NULL embryos are significantly smaller than controls, warranting testing for apoptosis through TUNNEL assay or caspase-3 staining, or proliferation assay through phospho-histone H3, to label mitotic cells.

H3.3-G34R NCC and HEMI-H3.3A embryos were comparable to controls in craniofacial cartilage and bone while H3.3-G34R embryos showed reduction of cartilage and ossification of bones.

We mated our *H3f3a*$^{LoxP/+}$ (HEMI-H3.3A) mice to *Wnt1-Cre2* transgenic mice to express the H3.3-G34R in neural crest cells. H3.3-G34R NCC embryos showed no difference between control embryos. Furthermore, the live H3.3-G34R NCC mice that were born were also comparable to control mice, viable and able to reproduce. These results suggest that mutant H3.3-G34R expression specifically in neural crest cells does not affect embryonic or postnatal development.

Constitutive HET G34R embryos showed reduction of cartilage and ossification of bones in E14.5 and E17.5 embryos, and the proportion of embryos with defects was significantly different from controls (Figure 3.11, 3.12). The fact that HEMI-H3.3A embryos showed no defects while constitutive HET G34R mutants did, supports H3.3-G34R is a gain of function mutation that is dominant negative in nature. Constitutive HOMO G34R mutants had similar phenotypes to HET G34R embryos, though z scores comparing the proportion of embryos with defects (3/5) to controls ($p=0.073$), was not significant. This result may be explained by the lower number of embryos generated and used for analysis with this genotype (N=5). More HOMO G34R mutants must be produced to confirm. Interestingly enough, constitutive expression of H3.3-G34R resulted in a decrease of only NCC-derived head bones and cartilage (Figure 3.13). Suggesting it is the expression of H3.3-G34R in all cells, which contributes to the observed phenotypes. More specifically, it supports that H3.3-G34R expression may be disrupting the extrinsic

environmental signalling the NCCs receive from surrounding tissues (from either the ectoderm, mesoderm, or endoderm), preventing their migration and/or differentiation.

NCC are governed by a complex of regulatory genes that equip them with their multipotency and migratory capabilities as well as control their patterning and differentiation. As previously stated, NCCs receive extrinsic environmental signals from the mesoderm and endoderm and this signalling is involved in directing the NCCs to their designated location and ensuring their proper development (Frisdal & Trainor, 2014). Migration is dictated by ephrin/Eph and Sdf1/Cxcr4 signalling proteins in addition to semaphore signalling proteins. Downstream of growth factors, numerous families of transcription factors are activated, including the Snail family (Snail1 and Snail2/Slug), SoxE family (Sox8, 9 and 10), Pax family (Pax3, 7) and Msx family (Msx1 and 2). In a cascade-like action these transcription factors, through feedback regulation, control the processes of neural crest development including specification, epithelial-to-mesenchymal transition (EMT), group cell migration and differentiation. Together they ensure that neural crest cells develop in a specific temporal and spatial manner, differentiating into the correct cell type respective to its designated tissue environment (Tien et al., 2015; Bhatt et al., 2013; Ansari, 2019). Fate regulation, localization, and patterning of NCCs, have been shown to be synchronized by multiple signaling pathways and factors. Some include: bone morphogenetic proteins (BMPs), wingless (Wnt), sonic hedgehog (Shh), Notch, retinoic acid signalling, distal-less (Dll) homeobox genes, endothelin-1 (ET-1), fibroblast growth factors (FGFs), epidermal growth factor (EGF), transforming growth factor β (TGFβ), transforming growth factor alpha (TGFα), and Twist-related protein (Twist) (Jeong et al., 2004; Costa et al., 2012; Minoux and Rijli, 2010; Francis-West et al., 1998). Factors arise directly from NCCs, facilitating communication between them, as well as from proximal cells of endodermal or mesodermal origins. For example, *Twist* is expressed in both the mesodermal core and mesenchyme of the pharyngeal arches. *Twist* is necessary for establishment of mesoderm/neural crest ectoderm boundaries and its removal in mice results in aberrant invasion of NCC into the paraxial mesoderm (Kindberg & Bush, 2019; Bildsoe et al., 2013). *Twist* expression together with mesodermal and endodermal pouch expression of *Tbx1,* facilitate proper segregation of pharyngeal arch 1 and 2 neural crest cell streams (Choe et al., 2014; Minoux & Rijili, 2010). *Tbx1* has also been supported to non-autonomously regulate NCC development, as it modulates expression of *Fgf8,* a protein expressed in the pharyngeal arches

crucial to NCC survival, as its removal results in significant neural crest cell apoptosis in pharyngeal arch 1 (Kindberg & Bush, 2019; Dunkel et al., 2020). The intricate reciprocal signaling occurring between the primary germ layers and neural crest cells is essential to NCC survival and development. Reductions in ossification could be due to programmed cell death or inhibition of signaling pathways important for osteogenesis. For example, Notch signaling allows for the differentiation of neural crest cells into osteoprogenitors. The TGFβ superfamily, which encompasses many growth and differentiation factors (including BMP), is responsible for regulating neural crest cell differentiation, necessary for the variety of cell-types that make up the elements of the face, including frontal bone osteoprogenitor cells and the palatal mesenchyme (Conway & Kaartinen, 2011; Siismets & Hatch, 2020).

Neural crest cells are dynamic throughout the process of differentiation and cells destined for different fates possess their own unique set of properties, varying with respect to the epigenetic marks they hold and genes they express. The amino terminal tail of histone H3.3 is highly conserved and extensively modified. Furthermore, it is commonly associated with active gene expression, readily associated with gene activating marks like H3K36me3 and H3K4me3. The role of the H3.3-G34R mutation in tumorigenesis and its mechanism of disruption in H3 function remains to be elucidated (Lowe et al., 2019). Glycine 34 is situated a mere four amino acids from the nucleosome core and is not a site of modification, but it is close to the modified site lysine 36 (K36). General consensus on the effect of the G34R mutation in cells is a slight decrease in K36me3 and slight increase in K27me3 (Lowe et al., 2019; Yadav et al., 2017; Jain et al., 2020; Lewis et al., 2013) (Figure 4.1).

Figure 4.1: Alteration of post-translational modifications in the G34R mutation. The G34R mutation is thought to block SETD2 activity, leading to a decrease in K36me3 (indicated by blue downwards arrow by K36 on right) and slight increase in K27me3 (blue upwards arrow by K27 left) in the affected histone tail.

Interestingly, decrease in H3K36 trimethylation is seen in patients with LLS syndrome, who harbour heterozygous mutations in SETD2, and some LLS patients present with skeletal dysplasia (Luscan et al., 2014; Lumish et al., 2015). Furthermore, K36 methylation is thought to be crucial in preventing premature expression of genes crucial to NCC development (Jacques-Fricke & Gammill, 2014) as well as splicing; both important processes for neural crest cell and craniofacial development (Beauchamp et al., 2020; Zaghi et al., 2020). There has also been proposal of the existence of a crosstalk between H3K36me3 and H3K27me3, suggesting they may have antagonistic roles, with H3K36 trimethylation antagonizing PRC2-mediated H3K27 trimethylation (Weng et al., 2014; Yuan et al., 2011). Without RNAseq and ChIPseq data to assess transcriptome changes or PTM patterns in our controls and mutants, we are limited in the conclusions we can draw in terms of their chromatin landscape. Phenotypes seen in our constitutive HET-G34R mutants may be a result of an increase in repressive marks and decrease in active marks that affect expression of genes necessary for NCC development. As proposed before, mutations occurring near the N-terminal tail may affect the protein-protein interactions of histone modifiers, disrupting their ability to deposit key PTMs that enact either the suppression or activation of gene expression programs necessary for development (Scwartzentruber et al., 2012l Wu et al., 2012; Bryant et al., 2020). More precisely, aberrant alteration in repressive and

activating marks may confer an inhibitory effect in NCC proliferation and/or differentiation, slowing the processes of chondrogenesis and osteogenesis in NCC-derived cartilages and bones, respectively.

CHAPTER V: CONCLUSION & FUTURE DIRECTIONS

Our data suggest that expression of H3.3- G34R in neural crest cells does not affect neural crest cell development or subsequent formation of the cartilage and skeletal elements of the head. Constitutive expression of H3.3-G34R, in all germ layers and their derivatives, led to hypoplasia of head cartilages and a reduction of head bone ossification in mice, supporting its current classification as a gain-of-function mutation. Knockout of *H3f3a* (H3.3A-NULL) mice were significantly smaller than controls and displayed severe reduction of cartilage and ossification in both neural crest and mesoderm derived head bones. Testing for increased apoptosis or decreased proliferation in cells of our H3.3-G34R constitutive and H3.3A-NULL mutants (through caspase-3 and phospho-histone H3 assay, respectively) could confirm if there is an increase in cell death or decrease in cell proliferation compared to controls. An additional measure that could be taken to further analyze craniofacial phenotypes would be measuring embryo head length, width, and height, to assess if there are significant differences between genotypes. Furthermore, cartilage/bone reduction in mutants could be quantified by calculating the area, followed by percent coverage, of Alcian Blue/Alizarin Red staining, using an image analysis program such as "*Image J"*. Finally, experiments such as Western blot analysis, RNAseq, and CHIPseq, must be conducted to elucidate whether there is reduction in nucleosomal incorporation of H3.3, changes in the cellular transcriptome, or altered histone tail modification. And more importantly, if these changes, in either gene expression or PTMs, are necessary for NCC development. Modification of H3.3 and its role in epigenetic regulation are rapidly developing fields, with new information being uncovered daily about the complex mechanisms of how they govern gene expression. Despite research efforts and advent of sophisticated technologies, we have only scratched the surface in the function of histone H3.3 modification, including its implication in development and misregulation in disease.

REFERENCES

Alberts, B., Johnson, A., Lewis, J., et al. 2002. Molecular Biology of the Cell. 4th edition. New York: Garland Science.

Allshire, R. C., Madhani, H. D., 2018. Ten principles of heterochromatin formation and function. Nature Reviews Molecular Cell Biology. 19, 229–244.

Ansari A, Bordoni B., 2020. Embryology, Face. In: StatPearls [Internet]. Treasure Island (FL): StatPearls Publishing.

Bannister, A. J., Kouzarides, T., 2011. Regulation of chromatin by histone modifications. Cell Res. 21, 381–395.

Beauchamp, M. C., Alam, S. S., Kumar, S., and Jerome-Majewska, L. A., 2020. Spliceosomopathies and neurocristopathies: two sides of the same coin?.Dev. Dyn. 249, 924–945.

Behjati, S., Tarpey, P. S., Presneau, N., Scheipl, S., Pillay, N., Van Loo, P., Wedge, D. C., Cooke, S. L., Gundem, G., Davies, H., Nik-Zainal, S., Martin, S., McLaren, S., Goodie, V., Robinson, B., Butler, A., Teague, J. W., Halai, D., Khatri, B., Myklebost, O., … Flanagan, A. M., 2013. Distinct H3F3A and H3F3B driver mutations define chondroblastoma and giant cell tumor of bone. Nature Genetics, 45, 1479–1482.

Benayoun, B. A., Pollina, E. A., Ucar, D., Mahmoudi, S., Karra, K., Wong, E. D., Devarajan, K., Daugherty, A. C., Kundaje, A. B., Mancini, E., Hitz, B. C., Gupta, R., Rando, T. A., Baker, J. C., Snyder, M. P., Cherry, J. M., & Brunet, A., 2014. H3K4me3 breadth is linked to cell identity and transcriptional consistency. Cell. 15*8*, 673–688.

Bhatt, S., Diaz, R., Trainor, P. A., 2013. Signals and switches in Mammalian neural crest cell differentiation. Cold Spring Harbor perspectives in biology, 5, a008326.

Bildsoe, H., Loebel, D. A., Jones, V. J., Hor, A. C., Braithwaite, A. W., Chen, Y. T., Behringer, R. R., Tam, P. P., 2013. The mesenchymal architecture of the cranial mesoderm of mouse embryos is disrupted by the loss of Twist1 function. Developmental biology. 374, 295–307.

Bolande, R.P., 1974. The neurocristopathies: a unifying concept of disease arising in neural crest maldevelopment. Hum. Pathol. 5, 409–429.

Bramlage, B., Kosciessa, U., Doenecke, D., 1997. Differential expression of the murine histone genes H3.3A and H3.3B. Differentiation. 62, 13–20.

Brioude, F., Toutain, A., Giabicani, E., Cottereau, E., Cormier-Daire, V., & Netchine, I., 2019. Overgrowth syndromes - clinical and molecular aspects and tumour risk. Nature reviews. Endocrinology. 15, 299–311.

Bryant, L., Li, D., Cox, S. G., Marchione, D., Joiner, E. F., Wilson, K., Janssen, K., Lee, P., March, M. E., Nair, D., Sherr, E., Fregeau, B., Wierenga, K. J., Wadley, A., Mancini, G., Powell-Hamilton, N., van de Kamp, J., Grebe, T., Dean, J., Ross, A., … Bhoj, E. J., 2020. Histone H3.3 beyond cancer: Germline mutations in Histone 3 Family 3A and 3Bcause a previously unidentified neurodegenerative disorder in 46 patients. Science advances. 6, eabc9207.

Bush, K. M., Yuen, B. T., Barrilleaux, B. L., Riggs, J. W., O'Geen, H., Cotterman, R. F., & Knoepfler, P. S., 2013. Endogenous mammalian histone H3.3 exhibits chromatin-related functions during development. Epigenetics & Chromatin. 6, 7.

Chapman S. C., 2011. Can you hear me now? Understanding vertebrate middle ear development. Frontiers in bioscience (Landmark edition). 16, 1675–1692.

Choe, C. P., & Crump, J. G., 2014. Tbx1 controls the morphogenesis of pharyngeal pouch epithelia through mesodermal Wnt11r and Fgf8a. Development.141, 3583–3593. Chromatin as the Whiteboard of Heart Disease. Circulation Research. 116, 1245-1253.

Cibi, D. M., Mia, M. M., Shekeran, S. G., Yun, L. S., Sandireddy, R., Gupta, P., Hota, M., Sun, L., Ghosh, S., 2019. Neural crest-specific deletion of *Rbfox2* in mice leads to craniofacial abnormalities including cleft palate. eLife. 8, e45418.

Cole, T. R., & Hughes, H. E., 1994. Sotos syndrome: a study of the diagnostic criteria and natural history. Journal of medical genetics, 31, 20–32.

Conway, S. J., & Kaartinen, V., 2011. TGFβ superfamily signaling in the neural crest lineage. Cell adhesion & migration. 5, 232–236.

Couldrey, C., Carlton, M. B., Nolan, P. M., Colledge, W. H., & Evans, M. J., 1999. A retroviral gene trap insertion into the histone 3.3A gene causes partial neonatal lethality, stunted growth, neuromuscular deficits and male sub-fertility in transgenic mice. Human molecular genetics. 8, 2489–2495.

Cox, S. G., Kim, H., Garnett, A. T., Medeiros, D. M., An, W., & Crump, J. G., 2012. An essential role of variant histone H3.3 for ectomesenchyme potential of the cranial neural crest. PLOS genetics. 8, e1002938.

Das, K. K., Kumar, R., 2017. Pediatric Glioblastoma. In: De Vleeschouwer S, editor. Glioblastoma [Internet]. Brisbane (AU): Codon Publications. Chapter 15.

Douglas, J., Hanks, S., Temple, I. K., Davies, S., Murray, A., Upadhyaya, M., Tomkins, S., Hughes, H. E., Cole, T. R., & Rahman, N., 2003. NSD1 mutations are the major cause of Sotos syndrome and occur in some cases of Weaver syndrome but are rare in other overgrowth phenotypes. American journal of human genetics. 72, 132–143.

Field. Y., Kaplan, N., Fondufe-Mittendorf, Y., Moore, I. K., Sharon, E., Lubling, Y., Widom, J., Segal, E., 2008. Distinct Modes of Regulation by Chromatin Encoded through Nucleosome Positioning Signals. PLOS Computational Biology. 4, e1000216.

Francis-West, P. H., Parish, J., Lee, K., Archer, C. W., 1999. BMP/GDF-signalling interactions during synovial joint development. Cell and Tissue Research. 296, 111–119.

Friedel, R. H., & Soriano, P., 2010. Gene trap mutagenesis in the mouse. Methods in enzymology. 477, 243–269.

Frisdal, A.,Trainor, P. A., 2014. Development and evolution of the pharyngeal apparatus. Wiley interdisciplinary reviews. Developmental biology. 3, 403–418.

Furukawa, A., Wakamori, M., Arimura, Y., Ohtomo, H., Tsunaka, Y., Kurumizaka, H., Umehara, T., Nishimura, Y., 2020. Acetylated histone H4 tail enhances histone H3 tail acetylation by altering their mutual dynamics in the nucleosome. Proceedings of the National Academy of Sciences of the United States of America. 117, 19661–19663.

Gibson, W. T., Hood, R. L., Zhan, S. H., Bulman, D. E., Fejes, A. P., Moore, R., Mungall, A. J., Eydoux, P., Babul-Hirji, R., An, J., Marra, M. A., FORGE Canada Consortium, Chitayat, D., Boycott, K. M., Weaver, D. D., & Jones, S. J., 2012. Mutations in EZH2 cause Weaver syndrome. American journal of human genetics. 90, 110–118.

Gillette, T.T., Hill, J. A., 2015. Readers, Writers, and Erasers: Chromatin as the Whiteboard of Heart Disease. Circulation Research. 116, 1245-1253.

Greer, E. L., Shi, Y., 2012. Histone methylation: a dynamic mark in health, disease and inheritance. Nature Reviews. Genetics. 13, 343–357.

Handy, D. E., Castro, R., Loscalzo, J., 2011. Epigenetic modifications: basic mechanisms and role in cardiovascular disease. Circulation. 123, 2145–2156.

Hödl, M., & Basler, K., 2009. Transcription in the absence of histone H3.3. Current Biology. 19, 1221–1226.

Hyun, K., Jeon, J., Park, K., Kim, J., 2017. Writing, erasing and reading histone lysine methylations. Experimental & Molecular Medicine. 49, e324.

Imaizumi, K., Kimura, J., Matsuo, M., Kurosawa, K., Masuno, M., Niikawa, N., & Kuroki, Y., 2002. Sotos syndrome associated with a de novo balanced reciprocal translocation t(5;8)(q35;q24.1). American journal of medical genetics. 107, 58–60.

Jacques-Fricke, B. T., Gammill, L. S., 2014. Neural crest specification and migration independently require NSD3-related lysine methyltransferase activity. Molecular biology of the cell. 25, 4174–4186.

Jain, S. U., Khazaei, S., Marchione, D. M., Lundgren, S. M., Wang, X., Weinberg, D. N., Deshmukh, S., Juretic, N., Lu, C., Allis, C. D., Garcia, B. A., Jabado, N., & Lewis, P. W., 2020. Histone H3.3 G34 mutations promote aberrant PRC2 activity and drive tumor progression. Proceedings of the National Academy of Sciences of the United States of America. 117, 27354–27364.

Jang, C. W., Shibata, Y., Starmer, J., Yee, D., & Magnuson, T., 2015. Histone H3.3 maintains genome integrity during mammalian development. Genes & Development. 29, 1377–1392.

Jeong, J., Mao, J., Tenzen, T., Kottmann, A. H., McMahon, A. P., 2004. Hedgehog signaling in the neural crest cells regulates the patterning and growth of facial primordia. Genes & Development. 18, 937–951.

Jegalian, B. G., De Robertis, E. M., 1992. Homeotic transformations in the mouse induced by overexpression of a human Hox3.3 transgene. Cell, 71, 901–910.

Kalashnikova, A. A., Rogge, R. A., Hansen, J. C., 2016. Linker histone H1 and protein-protein interactions. Biochimica et Biophysica Acta. 1859, 455–461.

Kamien, B., Ronan, A., Poke, G., Sinnerbrink, I., Baynam, G., Ward, M., Gibson, W. T., Dudding-Byth, T., & Scott, R. J., 2018. A Clinical Review of Generalized Overgrowth Syndromes in the Era of Massively Parallel Sequencing. Molecular Syndromology. 9, 70–82.

Kindberg A. A., Bush J. O., 2019. Cellular organization and boundary formation in craniofacial development. Genesis. 57:e23271.

Knight, R.D., Schilling, T,F., 2013. Cranial Neural Crest and Development of the Head Skeleton. In: Madame Curie Bioscience Database [Internet]. Austin (TX): Landes Bioscience.

Kornberg, R. D., 1974. Chromatin structure: a repeating unit of histones and DNA. Science. 184, 868–871.

Kuratani, S., 2018. The neural crest and origin of the neurocranium in vertebrates. Genesis. 56, e23213.

Kurotaki, N., Imaizumi, K., Harada, N., Masuno, M., Kondoh, T., Nagai, T., Ohashi, H., Naritomi, K., Tsukahara, M., Makita, Y., Sugimoto, T., Sonoda, T., Hasegawa, T., Chinen, Y., Tomita Ha, H. A., Kinoshita, A., Mizuguchi, T., Yoshiura Ki, K., Ohta, T., Kishino, T., … Matsumoto, N., 2002. Haploinsufficiency of NSD1 causes Sotos syndrome. Nature genetics. 30, 365–366.

Lewis, P. W., Müller, M. M., Koletsky, M. S., Cordero, F., Lin, S., Banaszynski, L. A., Garcia, B. A., Muir, T. W., Becher, O. J., & Allis, C. D., 2013. Inhibition of PRC2 activity by a gain-of-function H3 mutation found in pediatric glioblastoma. Science. 340, 857–861.

Lin, C. J., Koh, F. M., Wong, P., Conti, M., & Ramalho-Santos, M., 2014. Hira-mediated H3.3 incorporation is required for DNA replication and ribosomal RNA transcription in the mouse zygote. Developmental Cell. 30, 268–279

Lowe, B. R., Maxham, L. A., Hamey, J. J., Wilkins, M. R., & Partridge, J. F., 2019. Histone H3 Mutations: An Updated View of Their Role in Chromatin Deregulation and Cancer. Cancers. 11, 660.

Luger, K., Mader, A. W., Richmond, R. K., Sargent, D. F., Richmond, T. J., 1997. Crystal structure of the nucleosome core particle at 2.8 A resolution. Nature. 389, 251–260.

Lumish, H. S., Wynn, J., Devinsky, O., & Chung, W. K., 2015. Brief Report: SETD2 Mutation in a Child with Autism, Intellectual Disabilities and Epilepsy. Journal of autism and developmental disorders. 45, 3764–3770.

Luscan, A., Laurendeau, I., Malan, V., Francannet, C., Odent, S., Giuliano, F., Lacombe, D., Touraine, R., Vidaud, M., Pasmant, E., & Cormier-Daire, V., 2014. Mutations in SETD2 cause a novel overgrowth condition. Journal of medical genetics. 51, 512–517.

Maver, A., Čuturilo, G., Ruml, S. J., Peterlin, B., 2019. Clinical Next Generation Sequencing Reveals an H3F3A Gene as a New Potential Gene Candidate for Microcephaly Associated with Severe Developmental Delay, Intellectual Disability and Growth Retardation. Balkan journal of medical genetics: BJMG. 22, 65–68.

Mikkelsen, T. S., Ku, M., Jaffe, D. B., Issac, B., Lieberman, E., Giannoukos, G., Alvarez, P., Brockman, W., Kim, T. K., Koche, R. P., Lee, W., Mendenhall, E., O'Donovan, A., Presser, A., Russ, C., Xie, X., Meissner, A., Wernig, M., Jaenisch, R., Nusbaum, C., Bernstein, B. E., 2007. Genome-wide maps of chromatin state in pluripotent and lineage-committed cells. Nature. 448, 553–560.

Minoux, M., & Rijli, F. M., 2010. Molecular mechanisms of cranial neural crest cell migration and patterning in craniofacial development. Development. 137, 2605–2621.

Morrison, J. A., McLennan, R., Wolfe, L. A., Gogol, M. M., Meier, S., McKinney, M. C., Teddy, J. M., Holmes, L., Semerad, C. L., Box, A. C., Li, H., Hall, K. E., Perera, A. G., & Kulesa, P. M., 2017. Single-cell transcriptome analysis of avian neural crest migration reveals signatures of invasion and molecular transitions. eLife, 6, e28415.

Passarge, E., 1979. Emil Heitz and the concept of heterochromatin: longitudinal chromosome differentiation was recognized fifty years ago. Am. J. Hum. Genet. 31, 106 -115.

Peter, E., Larsen, D., 2004. Reconstruction of the Alveolar Cleft. Principles of Oral and Maxillofacial Surgery. Peterson's Principles of Oral & Maxillofacial Surgery 2nd ed.

Qiao, Q., Li, Y., Chen, Z., Wang, M., Reinberg, D., & Xu, R. M., 2011. The structure of NSD1 reveals an autoregulatory mechanism underlying histone H3K36 methylation. The Journal of Biological Chemistry. 286, 8361–8368.

Rigueur, D., Lyons, K. M., 2014. Whole-mount skeletal staining. Methods in molecular biology. 1130, 113–121.

Rio, M., Clech, L., Amiel, J., Faivre, L., Lyonnet, S., Le Merrer, M., Odent, S., Lacombe, D., Edery, P., Brauner, R., Raoul, O., Gosset, P., Prieur, M., Vekemans, M., Munnich, A., Colleaux, L., & Cormier-Daire, V., 2003. Spectrum of NSD1 mutations in Sotos and Weaver syndromes. Journal of medical genetics. 40, 436–440.

Sakai, A., Schwartz, B. E., Goldstein, S., Ahmad, K., 2009. Transcriptional and developmental functions of the H3.3 histone variant in Drosophila. Current Biology. 19, 1816–1820.

Sambrook, J., Fritsch, E. F., & Maniatis, T., 1989. Molecular cloning: A laboratory manual, 2nd edition. **Location: Cold Spring Harbor, N.Y.**

Schwartzentruber, J., Korshunov, A., Liu, X. Y., Jones, D. T., Pfaff, E., Jacob, K., Sturm, D., Fontebasso, A. M., Quang, D. A., Tönjes, M., Hovestadt, V., Albrecht, S., Kool, M., Nantel, A., Konermann, C., Lindroth, A., Jäger, N., Rausch, T., Ryzhova, M., Korbel, J. O., … Jabado, N., 2012. Driver mutations in histone H3.3 and chromatin remodelling genes in paediatric glioblastoma. Nature. 482, 226–231.

Shah, N., Sukumar, S., 2010. The Hox genes and their roles in oncogenesis. Nature Reviews Cancer. 10, 361–371.

Siismets, E. M., & Hatch, N. E., 2020. Cranial Neural Crest Cells and Their Role in the Pathogenesis of Craniofacial Anomalies and Coronal Craniosynostosis. Journal of developmental biology. 8, 18.

Simões-Costa, M. S., McKeown, S. J., Tan-Cabugao, J., Sauka-Spengler, T., Bronner, M. E., 2012. Dynamic and differential regulation of stem cell factor FoxD3 in the neural crest is Encrypted in the genome. PLoS genetics, 8, e1003142.

Simó-Riudalbas, L., Esteller, M., 2015. Targeting the histone orthography of cancer: drugs for writers, erasers and readers. British Journal of Pharmacology. 172, 2716–2732.

Sims, R. J., Nishioka, K., Reinberg, D., 2003. Histone lysine methylation: a signature for chromatin function. Trends Genet. 19, 629–639.

Sotos, J. F., Dodge, P. R., Muirhead, D., Crawford, J. D., & Talbot, N. B., 1964. Cerebral gigantism in childhood. a syndrome of excessively rapid growth and acromegalic features and a nonprogressive neurologic disorder. The New England journal of Medicine. 271, 109–116.

Srinivasan, A., Toh, Y. C., 2019. Human Pluripotent Stem Cell-Derived Neural Crest Cells for Tissue Regeneration and Disease Modeling. Frontiers Molecular Neuroscience. 12, 39.

Streubel, G., Watson, A., Jammula, S. G., Scelfo, A., Fitzpatrick, D. J., Oliviero, G., McCole, R., Conway, E., Glancy, E., Negri, G. L., Dillon, E., Wynne, K., Pasini, D., Krogan, N. J., Bracken, A. P., & Cagney, G., 2018. The H3K36me2 Methyltransferase Nsd1 Demarcates PRC2-Mediated H3K27me2 and H3K27me3 Domains in Embryonic Stem Cells. Molecular Cell. 70, 371–379.e5.

Szenker, E., Ray-Gallet, D., Almouzni, G., 2011. The double face of the histone variant H3.3. Cell Research. 21, 421–434.

Tang, M. C., Jacobs, S. A., Mattiske, D. M., Soh, Y. M., Graham, A. N., Tran, A., Lim, S. L., Hudson, D. F., Kalitsis, P., O'Bryan, M. K., Wong, L. H., Mann, J. R., 2015. Contribution of the two genes encoding histone variant h3.3 to viability and fertility in mice. PLoS Genetics. 11, e1004964.

Tang, M. C., Jacobs, S. A., Wong, L. H., Mann, J. R., 2013. Conditional allelic replacement applied to genes encoding the histone variant H3.3 in the mouse. Genesis. 51, 142–146.

Tatton-Brown, K., & Rahman, N., 2013. The NSD1 and EZH2 overgrowth genes, similarities and differences. American journal of medical genetics. Part C, Seminars in medical genetics. 163, 86–91.

Thomas, J. O., Kornberg, R. D., 1975. An octamer of histones in chromatin and free in solution. Proceedings of the National Academy of Sciences of the United States of America. 72, 2626–2630.

Tien, C. L., Jones, A., Wang, H., Gerigk, M., Nozell, S., Chang, C., 2015. Snail2/Slug cooperates with Polycomb repressive complex 2 (PRC2) to regulate neural crest development. Development. 142, 722–731.

Tremethick, D. J., 2007. Higher-Order Structures of Chromatin: The Elusive 30 nm Fiber. Cell. 128, 651-654.

Otterloo, E., V., Williams, T., Artinger, K. B., 2017. The old and new face of craniofacial research: How animal models inform human craniofacial genetic and clinical data. Developmental biology. 415, 171-187.

van Rij, M. C., Hollink, I., Terhal, P. A., Kant, S. G., Ruivenkamp, C., van Haeringen, A., Kievit, J. A., & van Belzen, M. J., 2018. Two novel cases expanding the phenotype of SETD2-related overgrowth syndrome. American journal of medical genetics. Part A. 176, 1212–1215.

Waddington, C., 1942. Canalization of development and the inheritance of acquired characters. Nature. 150, 563–565.

Wang, W. D., Melville, D. B., Montero-Balaguer, M., Hatzopoulos, A. K., & Knapik, E. W., 2011. Tfap2a and Foxd3 regulate early steps in the development of the neural crest progenitor population. Developmental biology. 360, 173–185.

Weng, M., Yang, Y., Feng, H., Pan, Z., Shen, W. H., Zhu, Y., Dong, A., 2014. Histone chaperone ASF1 is involved in gene transcription activation in response to heat stress in Arabidopsis thaliana. Plant, cell & environment. 37, 2128–2138.

Wilkie, A., Morriss-Kay, G., 2001. Genetics of craniofacial development and malformation. Nature Reviews Genetics. 2**,** 458–468.

William, J., Serman, L. S., Potter, S., Scott, W. J., 2001. Facial and Palatal Development. Human Embryology Larsen 3rd Edition. p.352; 365-371; 398-404

Wolffe, A. P., Matzke, M. A., 1999. Epigenetics: regulation through repression. Science. 286, 481–486.

Wu, G., Broniscer, A., McEachron, T. A., Lu, C., Paugh, B. S., Becksfort, J., Qu, C., Ding, L., Huether, R., Parker, M., Zhang, J., Gajjar, A., Dyer, M. A., Mullighan, C. G., Gilbertson, R. J., Mardis, E. R., Wilson, R. K., Downing, J. R., Ellison, D. W., Zhang, J., 2012. Somatic histone H3 alterations in pediatric diffuse intrinsic pontine gliomas and non-brainstem glioblastomas. Nature Genetics. 44, 251–253.

Xu, Y. M., Du, J. Y., Lau, A. T., 2014. Posttranslational modifications of human histone H3: an update. Proteomics, 14, 2047–2060.

Yadav, R. K., Jablonowski, C. M., Fernandez, A. G., Lowe, B. R., Henry, R. A., Finkelstein, D., Barnum, K. J., Pidoux, A. L., Kuo, Y. M., Huang, J., O'Connell, M. J., Andrews, A. J., Onar-Thomas, A., Allshire, R. C., & Partridge, J. F., 2017. Histone H3G34R mutation causes replication stress, homologous recombination defects and genomic instability in *S.pombe*. eLife, 6, e27406.

Yoon, A. J., Pham, B. N., Dipple, K. M., 2016. Genetic Screening in Patients with Craniofacial Malformations. Journal of Pediatric Genetics. 5, 220–224.

Yuan, W., Xu, M., Huang, C., Liu, N., Chen, S., & Zhu, B., 2011. H3K36 methylation antagonizes PRC2-mediated H3K27 methylation. The Journal of biological chemistry. 286, 7983–7989.

Zaghi, M., Broccoli, V., Sessa, A., 2020. H3K36 Methylation in Neural Development and Associated Diseases. Frontiers in Genetics. 10, 1291.

Zhao, Y., Garcia, B. A., 2015. Comprehensive Catalog of Currently Documented Histone Modifications. Cold Spring Harbor Perspectives in Biology. 7, a025064.

Zheng, Y., Sweet, S. M., Popovic, R., Martinez-Garcia, E., Tipton, J. D., Thomas, P. M., Licht, J. D., & Kelleher, N. L., 2012. Total kinetic analysis reveals how combinatorial methylation patterns are established on lysines 27 and 36 of histone H3. Proceedings of the National Academy of Sciences of the United States of America. 109, 13549–13554.

APPENDIX

Supplementary Data

Table S1: Colony Generation

A) Genotypes generated in *H3f3a*$^{LoxP/+}$ with Wnt-1-Cre2 tg

Litter	*H3f3a*$^{+/+}$	*H3f3a*$^{+/+}$;Wnt1-Cre2	*H3f3a*$^{LoxP/+}$	*H3f3a*$^{LoxP/+}$;Wnt1-Cre2	TOTAL
1	5	2	3	1	11
2	2	0	5	5	12
Total	7	2	8	6	23

B) Genotypes generated in *H3f3a*$^{LoxP/+}$ with *H3f3a*$^{LoxP/+}$

Litter	*H3f3a*$^{+/+}$	*H3f3a*$^{LoxP/+}$	*H3f3a*$^{LoxP/LoxP}$	TOTAL
1	0	4	0	4
2	3	6	0	9
Total	3	10	0	13

C) Genotypes generated in *H3f3a*$^{LoxP/+}$;Wnt-1-Cre2 tg with *WT mice*

Litter	*H3f3a*$^{+/+}$	*H3f3a*$^{+/+}$;Wnt1-Cre2	*H3f3a*$^{LoxP/+}$	*H3f3a*$^{LoxP/+}$;Wnt1-Cre2	TOTAL
1	1	1	4	1	7
2	2	1	6	1	10
Total	3	2	10	2	17

Genotypes generated in *H3f3a*$^{LoxP/+}$ with *WT mice*

D)

Litter	*H3f3a*$^{+/+}$	*H3f3a*$^{LoxP/+}$	TOTAL
1	5	4	9

Table S2: Genotypes of Dissected Embryos

E14.5 Dissections

A) Genotypes generated in *H3f3a*$^{LoxP/+}$ with Wnt-1-Cre2 tg

Litter	*H3f3a*$^{+/+}$	*H3f3a*$^{+/+}$;Wnt1-Cre2	*H3f3a*$^{LoxP/+}$	*H3f3a*$^{LoxP/+}$;Wnt1-Cre2	Mosaic	TOTAL
1	4	1	2	2	0	9
2	3	0	6	1	1	11
Total	7	1	8	3	1	20

B) Breeding of *H3f3a*$^{LoxP/+}$;Wnt1-Cre2 with *H3f3a*$^{LoxP/+}$

Litter	*H3f3a*$^{+/+}$	*H3f3a*$^{+/+}$;Wnt1-Cre2	*H3f3a*$^{LoxP/+}$	*H3f3a*$^{LoxP/+}$;Wnt1-Cre2	*H3f3a*$^{LoxP/LoxP}$	*H3f3a*$^{LoxP/LoxP/+}$;Wnt1-Cre2	*H3f3a*$^{G34R/+}$	*H3f3a*$^{G34R/+}$; Wnt1-Cre2	*H3f3a*$^{G34R/G34R}$	*H3f3a*$^{G34R/G34R}$; Wnt1-Cre2	*H3f3a*$^{G34RLoxP/G34R}$; Wnt1-Cre2	NT	Mosaic	TOTAL
1	1	0	4	1	3	3	0	0	0	0	0	0	0	12
2	0	2	0	0	0	0	3	2	1	1	0	0	0	9
3	4	3	0	0	0	0	0	0	0	0	0	0	0	8
4	0	2	0	1	0	0	0	2	1	2	0	0	0	8
Total	5	7	4	2	3	3	3	4	2	3	0	0	0	36

Genotypes generated in E17.5 Dissections

C) Breeding of *H3f3a*$^{LoxP/+}$;Wnt1-Cre2 with *H3f3a*$^{LoxP/+}$

Litter	*H3f3a*$^{+/+}$	*H3f3a*$^{+/+}$;Wnt1-Cre2	*H3f3a*$^{LoxP/+}$	*H3f3a*$^{LoxP/+}$;Wnt1-Cre2	*H3f3a*$^{LoxP/LoxP}$	*H3f3a*$^{LoxP/LoxP/+}$;Wnt1-Cre2	*H3f3a*$^{G34R/+}$	*H3f3a*$^{G34R/+}$; Wnt1-Cre2	*H3f3a*$^{G34R/G34R}$	*H3f3a*$^{G34R/G34R}$; Wnt1-Cre2	*H3f3a*$^{LoxP/G34R}$; Wnt1-Cre2	NT	Mosaic	TOTAL
1 20	2	2	2	2	1(1)	0	0	0	0	0	0	0	0	9
2 71	1	1	3	3	1(1)	0	0	4	0	0	2	0	0	15
3 126	0	1	0	0	0	0	3	1	0	1	0	0	0	6
4 115	5	1	0	0	0	0	0	0	0	0	0	0	0	6
5 68	1(1)	3	0	1	0	0	0	2	2	0	0	0	0	9
6 19	0	2	1	0	7	1	0	0	0	0	0	1	0	12
Total	9	10	6	6	9	1	3	7	2	1	2	1	0	57

Table S3: Weights of Dissected Embryos

A) E14.5 Weights (g)

H3f3a$^{+/+}$	*H3f3a*$^{+/+}$;Wnt tg	*H3f3a*$^{LoxP/+}$	*H3f3a*$^{LoxP/+}$;Wnt tg	*H3f3a*$^{G34R/+}$	*H3f3a*$^{G34R/+}$;Wnt tg	*H3f3a*$^{G34R/G34R}$	*H3f3a*$^{G34R/G34R}$;Wnt tg	Mosaic	*H3f3a*$^{LoxP/LoxP}$
0.24	0.311	0.19	0.203					0.32	
0.28	0.276	0.16	0.21	0.16	0.264	0.279	0.284		
0.27	0.17	0.39	0.19						
0.23	0.16	0.39	0.38	0.16	0.255	0.16	0.261		
0.19	0.3	0.37	0.24						
0.19	0.27	0.41		0.17	0.15		0.18		
0.18	0.26	0.38							
0.21	0.2	0.38			0.17				
0.36		0.34							
0.32		0.21							
0.34		0.27							
0.29		0.29							

B) E17.5 Weights (g)

H3f3a$^{+/+}$	*H3f3a*$^{+/+}$;Wnt tg	*H3f3a*$^{LoxP/+}$	*H3f3a*$^{LoxP/+}$;Wnt tg	*H3f3a*$^{G34R/+}$	*H3f3a*$^{G34R/+}$;Wnt tg	*H3f3a*$^{G34R/G34R}$	*H3f3a*$^{G34R/G34R}$;Wnt tg	*H3f3a*$^{LoxP/LoxP}$	*H3f3a*$^{G34R/LoxP}$;Wnt tg
1.16	0.76	0.587	0.86					0.718	0.85
1.33	1.33	0.94	1.52	0.909	0.941	1.41	1.061	0.573	0.8
1.17	1.38	0.91	0.97	1.194	0.86	1.31		0.616	
1.12	1.42	0.89	0.83	1.04	0.95			0.707	
1.16	0.661	0.84	0.9	1.49	0.92			0.743	
0.74	0.631	0.79	0.84	1.27	0.77			0.749	
0.81	1.15							0.692	
	1.214								
	0.92								
	0.81								

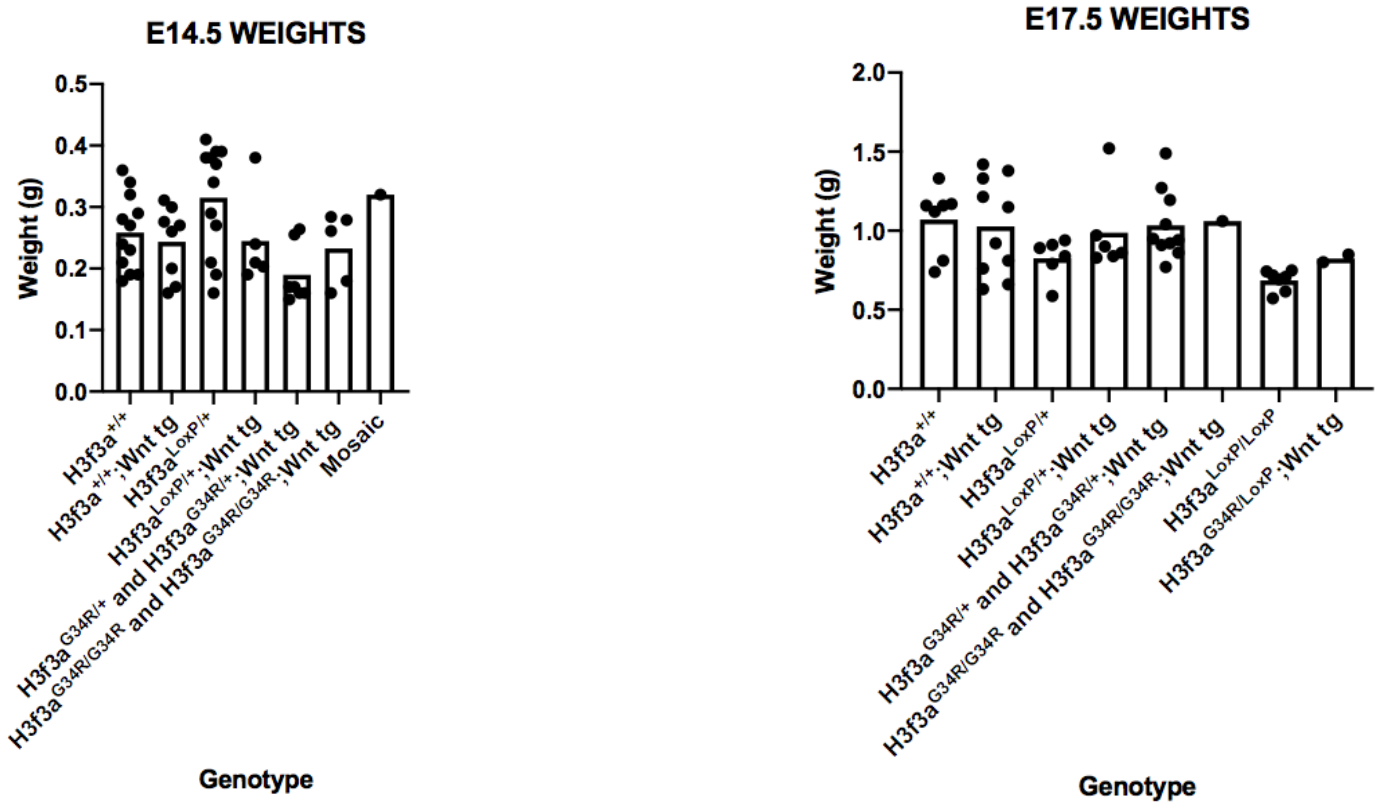

Supplementary Figure 1: Weight distribution across all genotypes generated in E14.5 and E17.5 dissections. Embryos were weighed upon removal from the yolk sac. Genotypes are plotted with embryo weight in grams. Data point represents one embryo.

Table S4: E14.5 ANOVA & Tukey HSD

A)

Treatment	Genotype
T1	Controls
T2	Hemi-H3.3A
T3	Heterozygous NCC
T4	Constitutive Heterozygous
T5	Constitutive Homozygous

Summary of Data

	Treatments					
	1	2	3	4	5	Total
N	20	12	5	7	5	49
∑X	5.047	3.78	1.223	1.329	1.164	12.543
Mean	0.2524	0.315	0.2446	0.1899	0.2328	0.256
$\sum X^2$	1.3401	1.2764	0.3234	0.2662	0.2846	3.4907
Std.Dev.	0.0592	0.0883	0.0779	0.0481	0.0584	0.0764

Result Details

Source	*SS*	*df*	*MS*	
Between-treatments	0.076	4	0.019	$F = 4.09845$
Within-treatments	0.204	44	0.0046	
Total	0.28	48		

The f-ratio value is 4.09845. The p-value is .006569. The result is significant at p < .05

B)

Pairwise Comparisons		$HSD_{.05} = 0.1007$ $HSD_{.01} = 0.1227$	$Q_{.05} = 4.0222$ $Q_{.01} = 4.8996$
T_1:T_2	$M_1 = 0.25$ $M_2 = 0.32$	0.06	Q = 2.50 (*p* = .40481)
T_1:T_3	$M_1 = 0.25$ $M_3 = 0.24$	0.01	Q = 0.31 (*p* = .99946)
T_1:T_4	$M_1 = 0.25$ $M_4 = 0.19$	0.06	Q = 2.50 (*p* = .40643)
T_1:T_5	$M_1 = 0.25$ $M_5 = 0.23$	0.02	Q = 0.78 (*p* = .98093)
T_2:T_3	$M_2 = 0.32$ $M_3 = 0.24$	0.07	Q = 2.81 (*p* = .28862)
T_2:T_4	$M_2 = 0.32$ $M_4 = 0.19$	0.13	Q = 5.00 (*p* = .00827)
T_2:T_5	$M_2 = 0.32$ $M_5 = 0.23$	0.08	Q = 3.28 (*p* = .15750)
T_3:T_4	$M_3 = 0.24$ $M_4 = 0.19$	0.05	Q = 2.18 (*p* = .53985)
T_3:T_5	$M_3 = 0.24$ $M_5 = 0.23$	0.01	Q = 0.47 (*p* = .99724)
T_4:T_5	$M_4 = 0.19$ $M_5 = 0.23$	0.04	Q = 1.71 (*p* = .74479)

Table S5: E17.5 ANOVA & Tukey HSD

A)

Treatment	Genotype
T1	Controls
T2	Hemi-H3.3A
T3	Heterozygous NCC
T4	Constitutive Heterozygous
T5	H3.3A-Null

The f-ratio value is 4.13671. The p-value is .006609. The result is significant at p < .05.

B)

Summary of Data						
	Treatments					
	1	2	3	4	5	Total
N	17	6	6	10	7	46
∑X	17.766	4.957	5.92	10.344	4.798	43.785
Mean	1.0451	0.8262	0.9867	1.0344	0.6854	0.952
$\sum X^2$	19.6883	4.1781	6.1954	11.1334	3.3151	44.5102
Std.Dev.	0.2648	0.1287	0.2662	0.2195	0.0663	0.2509

Result Details

Source	***SS***	***df***	***MS***	
Between-treatments	0.8148	4	0.2037	*F* = 4.13671
Within-treatments	2.0188	41	0.0492	
Total	2.8336	45		

Pairwise Comparisons		$HSD_{.05} = 0.3191$ $HSD_{.01} = 0.3893$	$Q_{.05} = 4.0346$ $Q_{.01} = 4.9224$
T_1:T_2	$M_1 = 1.05$ $M_2 = 0.83$	0.22	$Q = 2.77$ ($p = .30464$)
T_1:T_3	$M_1 = 1.05$ $M_3 = 0.99$	0.06	$Q = 0.74$ ($p = .98460$)
T_1:T_4	$M_1 = 1.05$ $M_4 = 1.03$	0.01	$Q = 0.14$ ($p = .99998$)
T_1:T_5	$M_1 = 1.05$ $M_5 = 0.69$	0.36	$Q = 4.55$ ($p = .02023$)
T_2:T_3	$M_2 = 0.83$ $M_3 = 0.99$	0.16	$Q = 2.03$ ($p = .60913$)
T_2:T_4	$M_2 = 0.83$ $M_4 = 1.03$	0.21	$Q = 2.63$ ($p = .35370$)
T_2:T_5	$M_2 = 0.83$ $M_5 = 0.69$	0.14	$Q = 1.78$ ($p = .71717$)
T_3:T_4	$M_3 = 0.99$ $M_4 = 1.03$	0.05	$Q = 0.60$ ($p = .99283$)
T_3:T_5	$M_3 = 0.99$ $M_5 = 0.69$	0.30	$Q = 3.81$ ($p = .07223$)
T_4:T_5	$M_4 = 1.03$ $M_5 = 0.69$	0.35	$Q = 4.41$ ($p = .02588$)